

General comments:

This manuscript analyzed the relationship of surface temperature with aerosol optical thickness (AOT) during a two-day smoke event. Some interesting results about operational forecast errors of surface temperature during this smoke event are presented. The authors attribute these forecast errors to missing aerosol radiative effects in the forecast models. However, the analysis is not convincing. The presentation needs some improvements.

We thank the reviewer for his/her constructive suggestions. We have taken the suggestions seriously and have carefully addressed the issues as shown below. The impact of smoke plumes to temperature forecasts has been documented in the past (also referenced in this paper). In fact, we are not the only one to notice the impact of smoke aerosols on surface temperatures for this smoke event. The local National Weather Service station has also recognized the issue and documented the potential impact of smoke plumes to temperature forecasts. For example, the Area forecast discussion issued by the Grand Forks NWS station at 10:00am CDT on June 29, 2015 mentions that “VERY THICK SMOKE TODAY WILL LIMIT TEMPERATURE RISE AT LEAST 2 TO 5 DEGREES...SO HAVE LOWERED TEMPS SOME AT LEAST. THIS IS VERY THICK SMOKE SO TEMPS COULD BE HELD DOWN INTO THE 70S...SO WILL MONITOR. THERE COULD BE SOME SHOWERS AND STORMS MAINLY EAST OF THE VALLEY THROUGH 00Z. OTHER THAN THE TEMP CHANGE...NO MAJOR CHANGES PLANNED TODAY.”

Major Comments:

1. The manuscript has a lot of descriptions of geographical locations, such as upper Midwest, Upper Mississippi, Ohio River Valley, etc. However, they are not identified on the figures. For readers who are not familiar with American geography, it is hard to follow the discussions.

Thanks for the suggestion. We have added a figure (now Figure 1), that provides a map of all of the geographic locations listed.

2. L372-375: Could you give some discussion about the meaning of forcing efficiencies and their relationship with surface temperature?

As suggested, we have added the following discussion:

“Note that TOA (surface) aerosol forcing efficiency is defined as the amount of change in upward (downward) short-wave radiation at TOA (surface) for a unit change in AOT. Negative surface aerosol forcing efficiencies indicate a reduction in short-wave radiation reaching the surface and mostly likely linkage to a decrease in surface temperature.”

3. L377-380: Figure 1e shows several points of high AOT (>1) between Jun 29 and July 1 at Ames.

We have revised the sentence to:

“the averaged AOT (0.5 μm) is around 0.5 for the Ames site, whereas the averaged AOT (0.5 μm) for the other sites range from 0.8-1.4 (Table 2).”

4. Section 3.2 and section 3.3: As shown in Figure 3, the interested regions are covered by two different synoptic systems, high pressure system to the southwest of the plume and low pressure system to the northeast of the plume. The sharp gradient of surface temperature in the interested regions are mainly due to the difference of the synoptic systems. For discussing aerosol impacts on surface temperature, differences in dynamical environment must be considered.

We agree that differences in the dynamical environment should also be considered. Still, for this case, the approximated MODIS AOT (based on the nearest available MODIS data), at 17:45 UTC on June 29, 2015, is 0.35 over Bismarck and is 4.43 over Grand Forks. If we assume an average aerosol surface forcing efficiency of $-120 \text{ W m}^{-2} \tau_{500}^{-1}$ (e.g. Table 2), the difference in surface downward SW flux is $\sim 480 \text{ W m}^{-2}$ between Bismarck and Grand Forks (300km apart) due to the smoke plume alone, which will introduce a non-negligible difference in surface temperature.

In fact, we are not the only one to realize the impact of smoke plumes on surface temperature. The Area Forecast Discussion issued by the Grand Forks NWS station at 10:00am CDT on June 29, 2015 suggested that “VERY THICK SMOKE TODAY WILL LIMIT TEMPERATURE RISE AT LEAST 2 TO 5 DEGREES...SO HAVE LOWERED TEMPS SOME AT LEAST.”

Also, the near surface wind speed is around 4.6m/s over Grand Forks and is around 5m/s over Bismarck (based on METAR data), indicating that “the difference of the synoptic systems” may have a marginal impact to this study.

We agree that the dynamical environment could be a factor as well and thus we have added the discussion:

“Lastly, besides the aerosol direct surface cooling effects, surface temperatures could also be impacted by differences in dynamical environments, which adds uncertainties to the study.”

5. L434-436: How do you get these numbers of -5_C and $-1.5_C/_{550}$?

On a monthly average, for the daily maximum temperature, Bismarck was historically warmer than Grand Forks by $1.0 \pm 2.0^\circ \text{C}$ (June 15th - July 14th 2015, excluding June 29th), with a correlation of 0.90. On June 29th, a ~ 8 degree daily maximum temperature difference is found between Bismarck and Grand Forks (25.6°C and 33.3°C for Grand Forks and Bismarck). By considering the historical mean and standard deviation of the temperature difference between Bismarck and Grand Forks ($1.0 \pm 2.0^\circ \text{C}$), it is approximated that the smoke plume introduced a ~ 5 degree difference in the daily maximum temperature between the two cities.

The daily mean AERONET AOT is around 3.4 (0.55 μm) over Grand Forks and the approximated MODIS AOT over Bismarck is 0.35 (0.55 μm , no AERONET data available), and

by dividing -5 degrees with the AOT difference of ~3 gives us the approximated aerosol cooling efficiency of $\sim -1.5^{\circ}\text{C}/\tau_{550}$.

6. L467-469: *Will this assumption induce bias in AOT?*

This assumption could introduce a bias in AOT. We have revised the paper to document this. “Note that this assumption may introduce a bias in the estimated MODIS AOTs.”

7. Section 3.4: *Similar to comment 4, will smoke Aerosol Direct Surface Cooling Efficiency be different in different dynamic environment? Also, studies have shown that aerosols can change thermodynamic environment or change cloud formation (as some clouds shown on Figure 6c and 6d), resulting in differences on model forecasts. Will these aerosol effects contribute to biased model forecasts on surface temperature?*

We believe the smoke Aerosol Direct Surface Cooling Efficiency may also be a function of different dynamic environments. However, to draw a conclusion, more than one case study is needed to categorize the Aerosol Direct Surface Cooling Efficiency under different dynamic environments, which is beyond the scope of this study. Still, we have mentioned the potential impact of dynamic environments in this paper as suggested from the response to comment 4.

In this paper, only the smoke Aerosol Direct Surface Cooling effect, which is the change in surface temperature due to smoke induced reduction in surface SW downward radiation, is studied. As the reviewer mentioned, aerosol particles can affect surface temperature indirectly through methods such as modifying cloud properties (e.g. Tao et al., 2012), however, these effects are beyond the scope of the study. But this is a legitimate point and we have added the following discussion to reflect the issue.

“Note that this study is focused on cloud free conditions and only the direct smoke aerosol surface cooling effect is studied. Still, aerosol particles may indirectly affect weather by altering cloud microphysics in both strati-form and convective clouds (e.g. Tao et al., 2012). Such effects warrant further discussions and evaluations.”

Minor comments:

1. L113-115: *Any references?*

We have added two references: Robock 1991; Mulcahy et al., 2014

2. L137-151: *The WRF-Chem model has been extensively used in weather research and forecasting. Some references, such as Chapman et al. [2009, ACP] and Grell et al. [2011, ACP], can be cited.*

We have added the discussion accordingly.

“some earlier studies have used WRF-Chem for aerosol related weather research and forecasting (e.g. Chapman et al. 2009; Grell et al. 2011).”

3. *L162-165: What’s the MODIS AOT at Grand Forks?*

The approximated MODIS AOT, based on the nearest available retrieval method as mentioned in the paper, is 4.3 (0.55 μ m).

4. *L224-229: A scatter plot between AERONET and MODIS may help.*

We didn’t add the plot, as evaluating the MODIS AOT product is not the focus of the paper and such effects have been documented in a few of our previous papers (Zhang and Reid, 2006; Shi et al., 2011; Hyer et al., 2011).

Shi, Y., Zhang, J., Reid, J. S., Holben, B., Hyer, E. J., and Curtis, C.: An analysis of the collection 5 MODIS over-ocean aerosol optical depth product for its implication in aerosol assimilation, *Atmos. Chem. Phys.*, 11, 557-565, doi:10.5194/acp-11-557-2011, 2011.

Hyer, E. J., Reid, J. S., and Zhang, J.: An over-land aerosol optical depth data set for data assimilation by filtering, correction, and aggregation of MODIS Collection 5 optical depth retrievals, *Atmos. Meas. Tech.*, 4, 379-408, doi:10.5194/amt-4-379-2011, 2011.

Zhang, J. and Reid, J.S., MODIS Aerosol Product Analysis for Data Assimilation: Assessment of Level 2 Aerosol Optical Thickness Retrievals, *J. Geophysical Research-Atmospheres*, VOL. 111, D22207, doi:10.1029/2005JD006898, 2006.

5. *L240-248 is similar to L251-260. It is better to combine these two paragraphs.*

L240-248 refers to data from the National Weather Service. L251-260 refers to data from the Automated Surface Observing System. Data reported from the NWS may include data from the ASOS stations. But to be clear with the data sources, we reported them separately.

6. *L267-269: Confused. Please reword.*

We have revised the sentence to:

“2 m surface temperature forecasts for the 18:00 Z valid times (30 and 54 hour forecasts) were examined.”

7. *L281: “at 18:00 UTC”?*

Yes, and we have modified the text accordingly.

8. *Should L288-293 be inserted to L282?*

We believe this is a writing style related issue and thus we didn't make changes.

9. *L323: "500 hPa" or "700 hPa"?*

We believe this is related to the statement "...winds that were west-northwesterly veering to north-north west at 500 hPa (see the 700 hPa height and wind analysis from the ECMWF reanalysis in Figure 3)." To prevent misinterpretation, the sentence is now modified to:

"The rapid transport of this smoke event was related to a persistent longwave high over the western United States, and corresponding trough over the eastern seaboard. The resulting in lower free tropospheric winds were west-northwesterly (e.g. see 700 hPa height and wind analysis from the ECMWF reanalysis in Figure 4 (note, new figure numbering). These winds veered to north-north west at 500 hPa."

10. *L326: The color bar of wind speed in Figure 3 has a maximum of 20 m/s.*

Yes. This is for 700 hPa. Wind speeds are higher at higher levels.

11. *L335: "500 hPa" or "700 hPa"?*

500 hPa. For brevity we showed 700 hPa in Figure 3, as representative of the lower free troposphere. But in the text we do discuss other levels.

12. *L367-368: For this smoke event?*

Yes.

13. *L376-377: Which time are the outliers are at? Are the outlier retrievals just for surface forcing efficiencies, or also including AOT, SSA etc.?*

These were listed on Table 2. It was high on downward surface forcing, and low on single scattering albedo and size. To reinforce the point we made regarding the potential sampling bias in the region, we now list the AOT values for the retrievals in Table 2 as well.

14. *L571: Isn't C_{scat} the same under similar conditions? Why should we expect different C_{scat} for lower aerosol loading?*

We have removed ", as well as a lower aerosol loading" as suggested.

General comments:

This study analyzed a major continental scale biomass burning smoke event to evaluate the degree of surface cooling introduced by the smoke plume, and how this affects model bias in near surface air temperature forecasts. The study found that the smoke aerosol induced surface cooling is comparable to model uncertainties, and thus concluded that incorporating a more realistic aerosol field into numerical model will not significantly improve the accuracy of near surface air temperature forecasts. The analysis is detailed, and the presentation is clear. However, the limitations of the study are not fully addressed and thus the conclusion is overstated. The length of the paper could also be shortened by making the description of the dataset and the event more concise, so that the reader could get to the key points more quickly.

We thank the reviewer for his/her thoughtful suggestions. We have revised the paper accordingly. Also, we have provided lengthy discussions of the event, as this sets up the basis for both this paper and a companion paper that we are currently working on.

Major comments:

The study is only focused on cloud free conditions, thus only aerosol direct effect is considered. However, it is well known that aerosols not only affect climate directly through reflecting or absorbing solar radiation, but also indirectly through affecting cloud microphysics in both stratiform and convective clouds. A summary of these effects could be found in Tao et al. (2012). With this effect omitted from the study, it is not justified to conclude that incorporating a more realistic aerosol field into numerical models will not significantly improve forecast accuracy. The limitations of the study should be addressed.

Thanks for the excellent suggestion. We have added the following discussion to reflect the issue.

“Note that this study is focused on cloud free conditions and only the direct smoke aerosol surface cooling effect is studied. Still, aerosol particles may indirectly affect weather by altering cloud microphysics in both strati-form and convective clouds (e.g. Tao et al., 2012). Such effects warrant further discussions and evaluations.”

Minor comments:

(1) Line 86-89: “Upscaling aerosol effects from individual weather phenomenon to climate: : :” The word “upscaling” seems to imply that the result from this study, which focuses on aerosol effect on weather, has implication for studies about aerosol effect on climate. This is misleading since whether the aerosol signal is detectable in weather forecasting does not relate to whether it is detectable in climate simulations. They are based on different time and spacial scales. I suggest to just focus this statement on studies of aerosol effect on weather phenomenon.

We agree with the reviewer that “aerosol signal is detectable in weather forecasting does not relate to whether it is detectable in climate simulations”. However, here “Upscaling” is used for

linking weather phenomena to climate in general and is not intended to imply the results of this study.

(2) Line 173: remove “the” after “a”.

Done.

(3) Line 281: remove “at”.

Done.

(4) Line 443: “temperate” should be “temperature”.

Done.

(5) Line 501: “52-hr” or “54-hr”? Some places are “52-hr”, while others are “54-hr” in the manuscript. It is also “54-hr” on the figure caption. This is confusing.

Changed from 52-hr to 54-hr.

(6) Line 509: Why does 30-hr forecast has larger error than 52-hr? From line 503, the largest surface temperature bias comes from 52-hr forecast.

This may relate to model uncertainties. Local-wise, it is not guaranteed that the 30-hr forecast is better than the 54-hr forecast in accuracy.

(7) Line 515: Should be “Figure A1 and A2”.

Done.

(8) Line 515: It seems the 0-hr forecast from NCEP has the largest error from Figure A2. This is different from ECMWF and UKMO, why?

Again, we suspect that this may be related to model uncertainties. However, exploring uncertainty sources in each model is beyond the scope of this paper.

(9) Line 541-545: It is not clear how this translates into the importance of radiative warming/cooling versus thermal advection.

To avoid confusion, we removed this sentence:

“Considering that the near surface air temperature is modulated by radiative warming/cooling and thermal advection, this result may suggest that radiative warming/cooling is more dominant for a colder region, which”

(10) Line 558-559: This sentence need to be re-written.

Done.

Reference: Tao, W.-K., J.-P. Chen, Z. Li, C. Wang, and C. Zhang (2012), Impact of aerosols on convective clouds and precipitation, *Rev. Geophys.*, 50, RG2001, doi:10.1029/2011RG000369.

1
2
3
4
5
6
7
8
9
10
11
12
13
14
15
16
17
18
19
20
21
22
23
24
25
26
27
28
29
30
31
32
33
34
35
36
37
38
39
40
41
42

An evaluation of the impact of aerosol particles on weather forecasts from a biomass burning aerosol event over the Midwestern US: Observational-based analysis of surface temperature

Jianglong Zhang¹, Jeffrey S. Reid², Matthew Christensen¹, and Angela Benedetti³

¹Department of Atmospheric Science, University of North Dakota, Grand Forks, ND

²Marine Meteorology Division, Naval Research Laboratory, Monterey, CA

³European Centre for Medium-Range Weather Forecasts, Reading, UK

Submitted to ACP

10 Dec. 2015

Corresponding Author Contact: Dr. Jianglong Zhang, c/o Department of Atmospheric Sciences,
4149 University Avenue Stop 9006, University of North Dakota, Grand Forks, ND, USA

E-mail: ijzhang@atmos.und.edu

Abstract

47
48
49 A major continental scale biomass burning smoke event from June 28-30, 2015, spanning central
50 Canada through the eastern seaboard of the United States, resulted in un-forecasted drops in
51 daytime high surface temperatures on the order of 2-5°C in the Upper Mid-West. This event,
52 with strong smoke gradients and largely cloud free conditions, provides a natural laboratory to
53 study how aerosol radiative effects may influence numerical weather prediction (NWP) forecast
54 outcomes. Here, we describe the nature of this smoke event and evaluate the differences in
55 observed near surface air temperatures between Bismarck (clear) and Grand Forks (overcast
56 smoke), to evaluate to what degree solar radiation forcing from a smoke plume introduces
57 daytime surface cooling, and how this affects model bias in forecasts and analyses. For this
58 event, mid-visible (550 nm) smoke aerosol optical thickness (AOT, τ) reached values above five.
59 A direct surface cooling efficiency of -1.5°C per unit AOT (at 550 nm, τ_{550}) was found. A
60 further analysis of European Center for Medium range Weather Forecasting (ECMWF), National
61 Centers for Environmental Prediction (NCEP), United Kingdom Meteorological Office (UKMO)
62 near surface air temperature forecasts for up to ~~542~~ hours as a function of Moderate Resolution
63 Imaging Spectroradiometer (MODIS) Dark Target AOT data across more than 400 surface
64 stations, also indicated the presence of the daytime aerosol direct cooling effect, but suggested a
65 smaller aerosol direct surface cooling efficiency with magnitude on the order of -0.25°C to -
66 1.0°C per unit τ_{550} . In addition, using observations from the surface stations, uncertainties in
67 near surface air temperatures from ECMWF, NCEP and UKMO model runs are estimated. This
68 study further suggests that significant daily changes in τ_{550} above 1, at which the smoke aerosol
69 induced direct surface cooling effect could be comparable in magnitude with model
70 uncertainties, are rare events on a global scale. Thus, incorporating a more realistic smoke

71 aerosol field into numerical models is currently less likely to significantly improve the accuracy
72 of near surface air temperature forecasts. However, regions such as East China, East Russian,
73 India and portions of the Saharan and Taklamakan deserts, where significant daily changes in
74 AOTs are more frequent, are likely to benefit from including an accurate aerosol analysis into
75 numerical weather forecasts.

76
77

78

79 **1 Introduction**

80 The impacts of aerosol particles on long-term climate variations have been extensively
81 studied from the standpoint of both their direct and indirect effects (e.g., IPCC, 2013). It is
82 frequently hypothesized that aerosol particles impart a radiative perturbation that ultimately can
83 alter overall atmospheric temperature, and consequently boundary layer and flow patterns (e.g.,
84 Cook and Haywood, 2004; Jacobson and Kaufman 2006; Lau and Kim 2006; Jacobson, 2014;
85 Tesfaye et al., 2015 to name a few). However, the climate impact of aerosol particles is derived
86 from a mosaic of individual aerosol events. Upscaling aerosol effects from individual weather
87 phenomenon to climate requires a thorough understanding of the nature of individual aerosol
88 events, how aerosol events relate to other meteorological forcing terms, and the data and model
89 tools used to diagnose outcomes. As one would expect, focus in the community has been
90 towards the direct radiative effects of either climatologically mean aerosol characteristics within
91 climate models, or, on the other extreme, large aerosol outbreaks where the aerosol signal is
92 hopefully clearer and more tractable. But even for severe events, diagnosing the extent of aerosol
93 radiative effects on “real meteorology” is a challenge. Due to model inadequacies, free running
94 models diverge from the true atmospheric state. NWP simulations, on the other hand, in part
95 compensate for aerosol radiative effects through the assimilation of copious amounts of
96 observations. Thus, one method for assessing aerosol impacts on weather is to utilize coupled
97 models or NWP forecasts themselves, searching for indicators of aerosol impacts in short to
98 medium range forecasts with well characterized initial conditions (e.g., Perez et al., 2006;
99 Chapman et al., 2009; Grell et al., 2011; Ge et al., 2014; Mulcahy et al., 2014; Kolusu et al.
100 2015; Remy et al., 2015).

Formatted: Font color: Red

101 Biomass burning plumes and airborne dust are attractive classes of phenomenon that lend
102 themselves to studies of how aerosol particle radiative effects can perturb the atmosphere.
103 Indeed, smoke and dust plumes can cover intercontinental scales with very high Aerosol Optical
104 Thickness (AOT, τ). Smoke is particularly amenable to natural laboratory studies as biomass
105 burning smoke, unlike dust, is largely a shortwave forcing agent and thus compensating
106 longwave effects are minimized. The plume nature of smoke also allows a certain degree of
107 control for underlying meteorology, and smoke production is not directly coupled to the
108 meteorology. Finally, smoke can display a range of absorption and thus can vary between being
109 a net warmer and net cooler of the local environment, yet maintain net cooling at the surface.
110 Indeed, effects of significant biomass burning events on local temperatures have long been
111 noted. Through analysis of several significant biomass-burning events, Robock (1991) showed a
112 1-7 °C decrease in near surface air temperature with a possible maximum decrease of 20°C, due
113 to smoke plumes. Using a numerical model, Westphal and Toon (1991) simulated the effects of
114 a massive 1982 fire deriving surface cooling of 8-10 °C. Other studies have also suggested
115 incorporating aerosol events in numerical weather models for more accurate weather forecasts
116 over aerosol contaminated regions (e.g. Robock 1991; Mulcahy et al., 2014).

117 Integrating aerosol events into weather prediction models has not been an easy task in the
118 past as aerosol particles have high variability in both spatial and temporal domains. Thus far
119 there has been little justification for the computational expense to include aerosol particle
120 radiative effects in operational simulations relative to other areas, such as cloud representation.
121 However, in recent years, break-through advancements have been made in both satellite aerosol
122 data and aerosol data assimilation, resulting in the development of both off and inline aerosol

123 models at NWP centers (e.g., Tanaka and Chiba, 2005; Zhang and Reid 2008; Benedetti et al.,
124 2009; Colarco et al., 2010; Perez et al., 2011; Kukkonen et al., 2012; Session et al., 2015).

125 From the point of view of satellite aerosol retrievals, regional and global aerosol events have
126 been routinely monitored with the use of both active and passive-based space borne sensors
127 including Moderate Resolution Imaging Spectroradiometer (MODIS), Multi-angle Imaging
128 SpectroRadiometer (MISR), and Cloud-Aerosol Lidar with Orthogonal Polarization (CALIOP)
129 on a daily basis (e.g. Levy et al., 2013; Kahn et al., 2010; Hsu et al., 2013). From the point of
130 view of modeling, advanced data assimilation schemes, including 2D/3D/4D-Var and Ensemble
131 Kalman Filter methods, have been applied to assimilate satellite and ground-based observations
132 (e.g. Zhang et al., 2008; 2011; 2014; Benedetti et al., 2009; Schutgens et al., 2010; Collins et al.
133 2001; Yu et al. 2003; Generoso et al. 2007; Adhikary et al. 2008; Tombette et al. 2009; Niu et al.
134 2008; Lin et al. 2008; Kahnert et al. 2008; Pagowski et al. 2012; Rubin et al., 2015). The
135 cumulative research progress in both observational and modeling based aerosol studies has
136 pushed the research front to the edge of fully incorporating prognostic aerosol fields into weather
137 forecasting models.

138 In realizing this potential, a few studies have attempted to incorporate advanced aerosol
139 schemes into numerical models for weather forecasting. For example, some earlier studies have
140 used WRF-Chem for aerosol related weather research and forecasting (e.g. Chapman et al. 2009;
141 Grell et al. 2011). Kolusu et al. (2015) studied the impact of biomass burning events on weather
142 forecasts with the use of the UK Met Office Unified Model. However, no significant
143 improvements were reported in weather forecasts after the inclusion of more complicated aerosol
144 representations (e.g. Mulcahy et al., 2014; Kolusu et al., 2015). Most recently, Remy et al.,
145 (2015) studied the radiative feedbacks of dust on boundary layer meteorology and found slight

Formatted: Font: Not Italic

146 improvements to surface temperature forecasts. The inability to significantly improve weather
147 forecasts via the incorporation of more realistic aerosol data in the forecasting processes from
148 these initial attempts could be from multiple causes. It is possible that improvements in both
149 quality and quantity of aerosol observations are needed. It is also possible that uncertainties
150 from other sources in traditional weather forecasts exceed the benefit of incorporating accurate
151 aerosol features in weather forecasting models. Also, for regions with persistent aerosol
152 contamination, the effect of aerosol particles on weather forecasts may already, in part, be
153 accounted for through assimilation of temperature data that are already affected by the direct
154 cooling effect of aerosol plumes.

155 In late June 2015, a rapidly evolving smoke aerosol event in the free troposphere, originating
156 from Canadian boreal fires, provided a near step function in fine mode Aerosol RObotic
157 NETwork (AERONET) 500 nm AOT (τ_{500}) from 0.1 to over 4 in the upper Midwestern United
158 States ([Figure 1 for a ~~Aqua MODIS RGB~~ Aqua MODIS RGB regional overview for the peak](#)
159 [of the event, Figure 4 ~~2~~, ~~MODIS RGB~~ or \(a\) \(d\) for a MODIS 4 day time series, and Figure 4\(e\)](#)
160 [for AERONET observations \(e\)](#)). This event, when coupled with operational NWP models,
161 provides a natural laboratory for the evaluation of the direct effect of aerosol particles on weather
162 forecasts. The abrupt increase in daily mean aerosol loading was not expected by either weather
163 forecasters or modelers, leading to a noticeable difference between forecasted and observed near
164 surface air temperatures for June 29&30 2015 as the largely cloud free smoke plume propagated
165 from Canada through the upper Midwest through the Ohio River Valley (Section 3 for details).
166 This event then provided pairs of sites experiencing low versus high AOT environments. For
167 example, while significant aerosol loading is reported from the Grand Forks AERONET station
168 ($\tau_{550} > 3$), Bismarck, only 300 km to the west experienced low to mild aerosol loading with τ_{550} of

169 ~0.1-0.4 as reported from the Collection 6 Terra MODIS Dark Target AOT data. The sharp
170 spatial gradient in aerosol loading makes this case an opportunity for further understanding the
171 effects of smoke aerosol particles on forecasts of surface temperature, and perhaps on any
172 downstream dependencies such as boundary layer height.

173 This paper is the first of two that explore the NWP implications of the June 29-30, 2015
174 biomass burning event. Here, we describe the nature of the event and demonstrate the daytime
175 direct cooling effect of smoke aerosol particles on the near surface air temperature forecasts.
176 This investigation then constrains a follow-up study using the ECMWF forecast model through
177 a) ~~the~~ quantification of the daytime direct aerosol effects as a function of altitude and aerosol
178 loading; b) establishment of the baseline uncertainties in the modeled near surface (1.5-m to 2-
179 m) air temperatures over the study domain; and c) investigation of the conditions under which
180 aerosol induced cooling effects can be strong enough to significantly alter upper air temperature
181 and downstream dynamical forecasts.

182 To meet these objectives, the impact of smoke aerosol particles on the European Center for
183 Medium range Weather Forecasting (ECMWF) 2-m air temperature forecasts and analyses are
184 studied and regions that could experience noticeable impacts of aerosols on weather forecasts are
185 explored. In addition, statistics are also generated for the National Centers for Environmental
186 Prediction (NCEP) and the United Kingdom Meteorological Office (UKMO) ensemble datasets.
187 This study is predominantly observational-based and describes the overall nature of the event
188 and the observed biases in NWP forecasts. In a companion paper, a sensitivity study using inline
189 simulations of the ECMWF forecast model is developed to further explore the impacts of smoke
190 aerosols on weather forecasts not only on surface temperatures, but also on any other potential

191 dynamical parameters such as predicted boundary layer height, and geopotential heights and
192 their gradient.

193

194 **2 Datasets**

195 This study focuses on the impact of the June 29th-30th smoke event on near-surface air
196 temperature forecasts from three numerical weather prediction models, ECMWF, NOAA NCEP
197 Global Ensemble Forecast System (GEFS), and UKMO Unified Model (UM). It includes their
198 comparison to Automated Surface Observing System (ASOS) surface data and National Weather
199 Service (NWS) forecasted temperature, controlled by AOT as derived from AERONET and
200 MODIS. The data are described below.

201

202 **2.1 Aerosol data**

203 Aerosol Optical Thickness (AOT) data over the study period are estimated from both
204 regional AERONET station data and Collection 6 (C6) Terra MODIS Dark Target (DT) aerosol
205 products (Levy et al., 2013). AERONET AOTs are derived from the measured solar energy at
206 seven wavelengths including 340, 380, 440, 500, 675, 870, 1020 and 1640 nm (Holben et al.,
207 1998). For the study period, quality assured Level 2.0 AERONET data are not available, and
208 thus the cloud-screened Level 1.5 AERONET data are used in this study. To derive fine mode
209 AOT associated with smoke and help remove any thin cirrus contamination that may be a
210 residual in the level 1.5 data, the Spectral Deconvolution Algorithm as described by O'Neill et
211 al. (2003) and verified by Chew et al., (2013) and Kaku et al. (2014), is utilized. Retrievals of
212 several aerosol-related parameters, including effective radius, spectral single scattering albedo

213 and upwelling and down-welling aerosol forcing efficiencies are also obtained from the
214 AERONET inversion products (Dubovik and King, 2000).

215 No AERONET data are available at the 550nm spectral channel. To be consistent with the
216 MODIS AOT data, AERONET τ_{550} are derived by interpolating AERONET AOTs reported at
217 the 500 and 675 μm channels using a method described in Shi et al., (2011). While there are a
218 number of AERONET sites installed in mid-to eastern United States, four observed the nature of
219 the plume particularly well: Grand Forks, North Dakota, (47.91° N, 97.33° W); Sioux Fall, South
220 Dakota (43.74°N, 96.63°N); Ames, Iowa (42.02°N, 93.77°W), and Bondville, Illinois (40.05°N,
221 88.37°W). These are labeled in Figure [1](#) and ~~and~~ [23](#)(a), (c), [7](#) & (e), with 500 nm fine mode
222 AOTs listed in Figure [42](#)(e).

223 Over land, MODIS DT aerosol data are available over dark surfaces such as non-desert
224 regions (Levy et al., 2013), and in this study, the Terra MODIS nadir 10-km resolution τ_{550}
225 retrievals are used, which best correspond to the midday 12:00 LST/18:00Z forecast period
226 evaluated. The accuracy of C6 MODIS AOT is reported to be on the order of $0.05+15\% \times \text{AOT}$
227 (Levy et al., 2013), although individual retrieval uncertainties may be higher (e.g. Shi et al.,
228 2011). As verification, Terra MODIS retrievals were compared to AERONET sites listed above
229 for the period of June 29th through, July 4th 2015, with five data points available at Grand Forks
230 having τ_{550} spanning from 0.88 to 3.7, three at Sioux Falls spanning 0.12 to 3.98, and one at
231 Ames with a τ_{550} of 0.58. Regression showed MODIS having a slight 10-20% high bias, and
232 outstanding regression coefficients ($r^2=0.98$). However, AOT retrievals failed for τ_{550} above ~4
233 due to saturation of the aerosol signal.

234

235 **2.2 Official forecast comparison**

236 The hypotheses developed for this effort originated from observations of significant
237 temperature forecast errors in the Dakotas in association with the central Canadian smoke plume.
238 Thus a key comparison for forecasted and observed daily maximum temperatures is performed
239 between Grand Forks (47.93°N, 97.03°W), in the center of the plume, and Bismarck (46.81°N,
240 100.78°W), 300 km to the west and outside of the plume. These sites are marked on Figure 23(a,
241 c). Official forecast data were obtained from the National Weather Service issued text weather
242 reports (Point Forecast Matrices and Climate Reports) from the Grand Forks and Bismarck, ND
243 stations respectively. The NWS Point Forecast Matrices include forecasted daily maximum
244 near-surface air temperatures and other weather conditions. The observed daily maximum
245 surface temperatures are obtained from the NWS Climate Reports which, per the ASOS Users'
246 Guide (<http://www.nws.noaa.gov/asos/aum-toc.pdf>, accessed on Oct. 29, 2015) have accuracy at
247 the half degree Celsius level. The archived NWS weather reports from June 15 - July 14, 2015
248 are obtained from the Iowa Environmental Mesonet (IEM) site
249 (<https://mesonet.agron.iastate.edu/>), which also hosts the NWS issued Morning Temperature and
250 Precipitation Summary, from which the observed daily maximum surface temperatures for
251 Roseau (48.85°N, 95.70°W) and Baudette (48.73°N, 94.62°W), MN were retrieved, as these
252 were not available from the NWS Climate Reports.

253

254 **2.3 Surface station data**

255 To supply surface observations for comparisons to forecast models over the greater Upper
256 Midwest and Upper Mississippi and Ohio River Valley study area, Automated Surface
257 Observing System (ASOS) surface data are obtained from the Iowa Environmental Mesonet
258 (IEM) site (<https://mesonet.agron.iastate.edu/>) for North Dakota, South Dakota, Nebraska,

259 Minnesota, Iowa, Alabama, Arkansas, Iowa, Illinois,, Indiana, Kansas, Kentucky, Missouri,
260 Mississippi, Nebraska, Oklahoma and Tennessee (Figures 23(a) and 23(e)). The ASOS data
261 include surface temperature (2m), dew point (2m), wind speed (10m) and direction (10m) as well
262 as visibility conditions. The surface temperature data used in study have the accuracy on the
263 order of 0.5°C for the normal temperature range of -50 to 50°C (ASOS user’s guide,
264 <http://www.nws.noaa.gov/asos/aum-toc.pdf>, accessed on Oct. 29, 2015).

265

266 **2.4 Forecast model data**

267 The next step in this analysis was to compare model midday (12:00-13:00 LST, 18:00Z)
268 surface temperature forecasts with ASOS observations, and relate differences to the location of
269 the smoke plume. 18:00 UTC was selected because it is near local noon and is only 15 minutes
270 off the Terra satellite overpass time (17:45 UTC) for North Dakota on June 29, 2015. The
271 primary model set used for comparison is the deterministic forecasts from ECMWF. 2 m surface
272 temperate forecasts for the 18:00 Z valid times (30 and 54~~2~~ hour forecasts) were examined ~~from~~
273 ~~the 12:00Z runs~~. The June 29th and 30th, 2015 18:00Z forecasts and ASOS observations are
274 examined in detail. Also examined are the forecast error statistics for these ASOS sites from
275 June 15 through July 14th.

276 Model data from the operational version of the European Centre for Medium Range Weather
277 Forecasts Integrated Forecast System (ECMWF IFS) were used. Forecast data are available
278 three-hourly from the 00 and 12UTC analysis. Analyses are also available at 06 and 18 UTC
279 from the four-dimensional variational (4D-Var) system with ensemble generated flow-dependent
280 background error statistics. The current resolution of the ECMWF IFS is approximately 16km

281 (T1279 spectral) with 137 vertical levels. More information are available here
282 <https://software.ecmwf.int/wiki/display/IFS/CY41R1+Official+IFS+Documentation>.

283 In addition to ECMWF, two other model data sets were also examined. Forecast surface
284 temperatures at 24-, 48-hour forecast intervals from the Global Ensemble forecast System
285 (GEFS) UKMO UM ensemble, ~~at~~ 18:00 UTC ~~at~~ were obtained from the THORPEX
286 Interactive Grand Global Ensemble (TIGGE) data archive (Bougeault et al., 2010). The NCEP
287 GEFS data are available on a global scale, with a $1 \times 1^\circ$ (Latitude/Longitude) spatial resolution
288 and 28 vertical layers at 00, 06, 12 and 18 UTC. Gridded statistical interpolation is included as
289 the data assimilation method for the control analysis (<http://tigge.ecmwf.int/models.html>). The
290 2-m air temperatures from the NCEP model runs are used. Note that the NCEP data record is
291 not complete for the selected study period, and missing data are listed in Table 1.

292 The UKMO data are available at a spatial resolution of $0.5555^\circ \times 0.8333^\circ$
293 (Latitude/Longitude) with a vertical resolution of 85 layers on a global scale. The 4D-Var
294 assimilation scheme is included for the control analysis (<http://tigge.ecmwf.int/models.html>).
295 The reported 1.5-m air temperature from the UKMO model runs are used in this study. Other
296 details of the UKMO and NCEP models can be found from Bougeault et al., (2010) and the
297 TIGGE web site (<http://tigge.ecmwf.int/models.html>).

298

299 ***2.5 Other data and metadata used in this analysis.***

300 To assist the analysis, data from a number of sources are utilized. Descriptions of fire
301 activity were obtained from the Canadian Interagency Forest Fire Center (CIFFC) situation
302 reports (<http://www.cifff.ca/>, last accessed 1 Dec., 2015). MODIS fire hotspot data were also
303 used (MOD35/MYD35, Justice et al., 2002). Soundings with temperatures, dew points, and

304 mixing ratios from radiosonde data at Aberdeen, SD are used (45.45N; 96.4W). To diagnose
305 low mid troposphere flow patterns, ECMWF reanalysis were utilized (Dee et al., 2011). Finally
306 to assess the transport trajectory of individual smoke parcels, The Hybrid Single-Particle
307 Lagrangian Integrated Trajectory (HYSPLIT) model (Draxler and Hass, 1997) is also used. The
308 HYSPLIT model computes trajectories of air parcels, both in forward and backward modes,
309 given the geolocation and altitude of an air parcel, as well as model initiation and spinning times.

310

311 **3. Results**

312 *3.1 General description of the June event*

313 The smoke event described here originated in a set of fires in Northwest Territories and
314 northern Alberta and Saskatchewan that were initiated ~June 23, 2015, as discussed by CIFFC
315 and observed in MODIS fire hotspot anomalies. These fires were likely the result of lighting in
316 association with widespread thunderstorm activity in central Canada lasting several days. By
317 June 27th, 2015 (Figure 42(a)), over 60 individual fires or complexes were visible in the MODIS
318 fire product, with over 30 fires reported greater than 1000 Ha by the CIFFC. June 28th, 2015
319 MODIS imagery (Figure 42(b)) showed significantly enhanced fire activity, with thick palls of
320 smoke being visible over central Canada. Comparison of MODIS fire to the CIFFC suggests that
321 a number of major fire complexes were missed in the satellite product, with significant burning
322 being missed in central Saskatchewan and Manitoba. Nevertheless the dense smoke was present.
323 By June 29th and 30th, smoke was clearly being transported across the Midwest, through the
324 Upper Mississippi and Ohio River Valleys, and into the Carolinas.

325 [The rapid transport of this smoke event was related to a persistent longwave high over the](#)
326 [western United States, and corresponding trough over the eastern seaboard. The resulting in](#)

Formatted: Indent: First line: 0.25", Line spacing: Double

327 [lower free tropospheric winds were west-northwesterly \(e.g. see 700 hPa height and wind](#)
328 [analysis from the ECMWF reanalysis in Figure 4\)](#). These winds veered to north-north west at
329 [500 hPa](#).

330 ~~The rapid transport of this smoke event was related to a persistent longwave high over the~~
331 ~~western United States, and corresponding trough over the eastern seaboard resulting in lower free~~
332 ~~tropospheric winds that were west-northwesterly veering to north-north west at 500 hPa (see the~~
333 ~~700 hPa height and wind analysis from the ECMWF reanalysis in Figure 3)~~. Thus, smoke was
334 channeled into the upper Midwest from central Canada. Smoke transport was further enhanced
335 by a fast moving shortwave and cold front, with 700 hPa winds at $\sim 25 \text{ m s}^{-1}$ (evident from the
336 upper Great Lakes through Iowa and Nebraska in Figure [34\(a\)](#)). This shortwave resulted in the
337 first tongue of smoke entering the US through central North and South Dakota on June 28th
338 (Figure [42\(b\)](#)). The most dramatic day, June 29th, 2105, saw the rapid transport of the major
339 smoke pall from northern Canada into the central Midwest behind the aforementioned shortwave
340 with mid visible AOTs in the upper Midwest above 4 (Figure [42\(c\)](#) & (e)). Embedded in this
341 smoke event were a set of smaller disturbances and associated wind enhancements across south
342 central Canada and the Upper Midwest (Figure [34\(b\)](#)). At the core 18:00Z analysis time for this
343 study, peak winds associated with the shortwave ranged from west-northwesterly 10 m s^{-1} at 950
344 hPa, veering to northwesterly to 25 m s^{-1} at 500 hPa.

345 A major shift in the pattern occurred on June 30th. Smoke from the previous day had now
346 advected into the Upper Mississippi and Ohio River Valley. Indeed, HYSPLIT trajectories
347 suggest smoke over Grand Forks should have advected to South Central Illinois within 24 hours.
348 At the same time, a low and occluded front moved into the Dakotas, bringing heavy cloud cover,
349 some rain, and more zonal winds (Figure [42\(d\)](#), Figure [34\(c\)](#)). At the same time, observed fire

350 activity diminished. Over the first week of July, while smoke was still clearly present at
351 moderately high levels in the upper Midwest (Figure 42(e)), the plume structure was not as
352 nearly dramatic. Smoke was also frequently embedded in cloud layers. By July 6th, a significant
353 cold front moved through the area, largely putting the smoke event to an end (e.g., Figure 42(e)).
354 From June 23- July 9, CIFFC reported that ~2,000,000 Ha were burned.

355 Operational radiosonde releases within the June 29-30 main smoke event are rare due to the
356 unfortunate trajectory of the main plume; perfectly in-between the Bismarck and International
357 Falls stations in the north and the Omaha/Topeka/Springfield corridor and
358 Chahassen/Davenport/Lincoln corridor in the south. Further, the 0Z and 12Z releases are
359 nominally in the morning and evening in the plume region. However, there were two
360 radiosondes related to the event, collected under cloud free sky conditions; the June 29 12:00 Z
361 and June 30 0:00 Z release at Aberdeen (Figure 45). Even though the site is on the edge of the
362 main plume, the MODIS inferred τ_{550} was still high ~2. Clearly, the soundings are dry, with
363 temperature and dew point profiles indicative of relative humidity on the order of 40-50%.
364 Water vapor mixing ratios dropped to below 2 g kg^{-1} , by 600 hPa, or 4 km.

365 Unfortunately for ascertaining plume altitudes for this event, no Cloud-Aerosol-Lidar with
366 Orthogonal Polarization (CALIOP) lidar data are available until June 30th due to solar flare
367 activity. Over the remaining days, orbit and clouds prevented clear operations across the axis of
368 the plume. However, we can infer from the early morning and afternoon July 1st overpasses over
369 the East coast that this plume was largely below 5 km in altitude. This is corroborated by the
370 Aberdeen sounding, which showed very low water vapor mixing ratios above 4 km in altitude.
371 In regard to smoke base, despite the very high AOTs, surface PM_{10} measurements hardly

372 registered the plume passage. Based on all of the above information we are confident that the
373 plume was confined to the lower to middle free troposphere.

374 Estimates of particle size and optical properties of the smoke plume were retrieved from the
375 four core AERONET sites used in this analysis (Table 2). These retrievals were collected from
376 June 29-July 3rd over the study area. Particle sizes were fairly stable over the United States, with
377 an effective radius of $\sim 0.165 \mu\text{m}$, or a volume median diameter of $\sim 0.38 \mu\text{m}$. This value is large
378 in comparison to more typical boreal fires (e.g., Reid et al., 2005), but well within values found
379 for mega events from Canada (e.g., 2002 Quebec fire with $\tau_{550} > 5$; Colarco et al. 2004; O'Neill
380 et al., 2005). Retrieved single scattering albedo was also consistent and within expected values,
381 ~ 0.94 in the mid visible. In regard to this analysis of surface temperature, what we are most
382 interested in is forcing efficiencies, which ranged from -48 to $-58 \text{ W m}^{-2} \tau_{550}^{-1}$ for the top of the
383 atmosphere. For retrieved surface forcing efficiencies, values varied more between sites. Grand
384 Forks, Sioux City and Bondville all agreed well, ranging from -118 to $-124 \text{ W m}^{-2} \tau_{550}^{-1}$. Note
385 that TOA (surface) aerosol forcing efficiency is defined as the amount of change in upward
386 (downward) short-wave radiation at TOA (surface) for a unit change in AOT. Negative surface
387 aerosol forcing efficiencies indicate a reduction in short-wave radiation reaching the surface and
388 mostly likely linkage to a decrease in surface temperature. However the Ames site had several
389 outlier retrievals leading to a higher magnitude downward forcing efficiency of $-165 \text{ W m}^{-2} \tau_{550}^{-1}$
390 ¹, ~~and due to noticeably~~ noticeably lower near infrared single scattering albedos and slightly
391 smaller size. This departure was consistent through the event. One explanation of this difference
392 between Ames versus other sites is that the averaged AOT ($0.5 \mu\text{m}$) is around 0.5 for the Ames
393 ~~siteno retrievals were made at Ames for τ_{550} higher than 0.65,~~ whereas the averaged AOT (0.5

394 μm) for the other sites range from 0.8-1.4 (Table 2)~~other sites had AOT's closer to 1.5.~~ Thus,
395 sampling bias is likely a factor.

396

397 **3.2 Observed temperature patterns in association with the June 29-30 event.**

398 Figures 23(a), (c), (e) show the RGB true color images of the smoke event over the upper
399 Midwestern US on June 28th (17:00 UTC) and June 29th (17:45 UTC), and over the Upper
400 Mississippi and Ohio River Valley on June 30th (16:50 + 16:55 UTC), constructed using the
401 Collection 6, Level 1b Terra MODIS data. Figures 23(b), (d), (f) show the corresponding Terra
402 MODIS level 2.0 DT τ_{550} for the same study periods as Figures 23(a), (c), (e). Over-plotted on
403 Figures 23(a), (c), (e) are the observed surface temperatures reported from ASOS stations from
404 North Dakota, South Dakota, Nebraska, Minnesota and Iowa on June 28th and June 29th, and
405 from Alabama, Arkansas, Iowa, Illinois, Indiana, Kansas, Kentucky, Missouri, Mississippi,
406 Nebraska, Oklahoma and Tennessee on June 30th. Each data point in Figs. 32(a), (c), (e)
407 represents the averaged observations within ± 10 minutes from 18:00 UTC of each given day for
408 a given station. The observations from 18:00 UTC are selected as both model analyses and
409 forecasts are available at this time enabling us to further explore differences in between modeled
410 and observed surface temperatures with respect to smoke aerosol properties.

411 Shown in Figure 23(a), on June 28th, a stripe of smoke aerosol plume starts to appear over the
412 upper Midwest region. The overall aerosol loadings are still relatively low ($\tau_{550} < 0.8$ for the
413 stripe of plume and less than 0.2 for most other regions) across the domain. A mild temperature
414 difference on the order of 1-2 °C is observed between Eastern and Western North Dakota. In-
415 comparison, on June 29th, a thick smoke plume is observed over the Eastern Dakotas and
416 Western Minnesota with significant MODIS DT τ_{550} values of 2-5. While warmer surface

417 temperatures of 27-32°C are observed over the Western Dakotas where lighter aerosol loadings
418 (less than 0.6) are found, surface temperatures of 22-24.5°C are found over the Eastern Dakotas
419 and Western Minnesota. The sharp spatial gradient in surface temperature on the order of 5°C in
420 between Eastern and Western North Dakota on June 29, 2015, matching the smoke plume
421 pattern, shows the potential influence of the smoke aerosol particles on the observed surface
422 temperatures.

423 On June 30th, the smoke plume migrates to the Upper Mississippi and Ohio River Valley, as
424 shown in Figs. 32e and 32f. Note that surface observations are obtained around 18:00 UTC, and
425 the Terra MODIS overpasses are 16:50-16:55 UTC. Thus, there is ~ one hour difference in
426 between surface- and satellite-based observations. Still, as shown in Figure 23(e), especially
427 over Missouri (Center of Figure 23(e)), lower surface temperatures are visible over regions with
428 heavy aerosol loadings, which again, reinforces the finding from the June 29th case.

429

430 ***3.3. Impacts of the smoke plume on an operational weather forecast***

431 To assess the degree to which the smoke event impacted forecast temperatures, we first
432 performed a hand analysis of the difference in forecast and observed surface temperatures
433 between Grand Forks and Bismarck as reported from the National Weather Service for June 29th.
434 These two sites correspond to the middle and just outside the main plume. Figure 5-6 shows the
435 forecast maximum surface air temperatures up to 96-hour for Grand Forks and Bismarck for June
436 29th, 2015. Filled stars represent forecast update time. The final daily maximum temperatures,
437 nominally 25.6°C and 33.3°C for Grand Forks and Bismarck respectively, are also shown. For
438 June 29th, an ~8°C difference is seen between sites in and out of the plume even though,
439 typically, the high temperatures between Grand Forks and Bismarck are highly correlated. For

440 the month surrounding the event (June 15th - July 14th, excluding June 29th), Bismarck was
441 historically warmer than Grand Forks by $1.0 \pm 2.0^\circ \text{C}$, with a correlation of 0.90. Forecasters are
442 well aware of this natural difference and hence account for it in their forecasts. It is also
443 noteworthy that while the daily maximum near surface air temperature forecasts for June 29th
444 remain unchanged since June 27th for Bismarck, the Grand Forks NWS made a -2.8°C (-5°F)
445 adjustment for their daily maximum near surface air temperature forecast at around 10:00 am
446 (local time) on June 29th, 2015, possibly to compensate for the initial unexpected surface cooling
447 due to the thick smoke aerosol plume. Despite the higher winds in the lower to mid free
448 troposphere, June 29th was a relatively calm day with moderate winds at the surface, ($\sim 3\text{-}5 \text{ m s}^{-1}$).
449 Taking all of the above factors into consideration, it is hypothesized that the smoke plume with
450 AERONET-reported daily mean τ_{550} of ~ 3.4 introduced a surface temperature cooling for Grand
451 Forks of $\sim 5^\circ \text{C}$. This is equivalent to a daytime aerosol cooling efficiency of $\sim -1.5^\circ \text{C}/\tau_{550}$, given
452 that the daily averaged τ_{550} is 3.4 as reported from Grand Forks AERONET station. Meanwhile,
453 the reported MODIS τ_{550} value over Bismarck was ~ 0.35 .

454 While observations from Bismarck and Grand Forks represents measurements at the diffuse
455 western edge and the central smoke plume, Roseau and Baudette, MN, which are close to Grand
456 Forks, are selected to represent the eastern diffuse edge of the smoke plume. As listed in Table
457 3, τ_{550} are 0.84 and 1.06 for Roseau and Baudette respectively at 17:45 UTC, June 29th, 2015, as
458 approximated from MODIS DT retrievals. Note that using the observed surface temperatureate
459 differences between Grand Forks and the two selected cities in MN for evaluating aerosol direct
460 cooling effect is not ideal, as surface temperatures from Roseau and Baudette may be also
461 modulated by nearby lakes. Further, lower correlations in daily maximum temperatures, around
462 0.75, are found between Grand Forks and the other two locations in MN. Still, Grand Forks is

463 around 2.5°C warmer than Roseau and Baudette on a monthly average (Table 3). However, on
464 June 29th, 2015, a much smaller temperature difference of 1.1°C is found in between Grand
465 Forks and Baudette, and Roseau is actually 0.6°C warmer than Grand Forks. Both cases may
466 indicate the potential smoke cooling effect. ~~Lastly, it~~ is noteworthy that the NWS made a -
467 1.7°C (-3°F) adjustment for the forecasted daily maximum temperatures on June 29th, 2015 for
468 both Roseau and Baudette, MN, possibly to compensate for the unexpected smoke aerosol
469 induced surface cooling. Lastly, besides the aerosol direct surface cooling effects, surface
470 temperatures could also be impacted by differences in dynamical environments, which adds
471 uncertainties to the study.

473 ***3.4. Impacts of the smoke plume on numerical model predictions***

474 The above hand analysis provides a benchmark estimate of the cooling efficiency of the
475 Canadian smoke plume. To test this value through an objective analysis, we compared this
476 finding to surface forecast errors focusing on the ECMWF models, starting with the June 29th
477 case. After this analysis, we extended the study to the NCEP and UKMO models and for the
478 June 30th case as well. A synopsis of findings is provided in Figure 67, where we show (a) the
479 relationship between recorded 18:00Z temperature to MODIS τ_{550} ; (b) the difference of ASOS
480 observation to ECMWF 30 hr. forecast against τ_{550} ; and (c) and (d), the corresponding overlay
481 of observation minus ECMWF 30 hr. forecast mapped over the June 29th and 30th investigation
482 domains. The plots are generated using measurements from ground stations as shown in Figures
483 2-3 (c) and 23(e). Also, over the center of the smoke aerosol polluted regions, the smoke plume
484 is so optically thick that the MODIS aerosol retrieval scheme failed to report τ_{550} values. Thus,
485 the closest MODIS τ_{550} value within 1° Latitude/Longitude of a given ground station is used to

486 represent the τ_{550} value of that station where there is no MODIS aerosol retrieval available. Note
487 that this assumption may introduce a bias in the estimated MODIS AOTs.

489 **3.4.1 The June 29th case**

490 The June 29th, 2015 case is an ideal case for studying the impact of the smoke plume on
491 numerical model forecasted near surface air temperatures for a few reasons. Firstly, both
492 surface and satellite observations are in close proximity in time (15 minutes) to the 18:00UTC
493 model forecasts and analysis. Secondly, the thick smoke plume is not expected by the model and
494 has not been accounted for in numerical model simulations.

495 Certainly over the region, there is a clear relationship between 18:00Z measured
496 temperature (T_{obs}) and MODIS τ_{550} (Figure 6a7a). In general, temperature is reduced by 1°C per
497 unit τ_{550} . However, there are exceptions, notably a drop in temperature for a cluster of data
498 points of at τ_{550} of ~ 1 . This group of data points belongs to sites on the eastern side of the June
499 29th Upper Midwest domain, associated with the great lakes and lake country of Wisconsin (as is
500 also evident in Figure 23). Thus, we must be careful to acknowledge that there is a natural
501 overall east to west positive temperature gradient on this day. Indeed, for the +/-15 day period
502 surrounding but excluding the event (Figure 2e3g), Wisconsin is generally 1-4 degrees cooler.
503 Excluding these cooler data points, the overall tendency is 1-2°C per unit τ_{550} . We consider this
504 1-2°C per unit τ_{550} set of values to be the range of observational sensitivity.

505 As the next step, we attempt to control for the gradient in temperature using the forecast
506 model itself. Figure 67(b) presents the ASOS 18Z observation minus the ECMWF 30 hr forecast
507 against MODIS τ_{550} . The values of this difference are also spatially mapped in Figure 67(c).
508 Here, in corroboration with the pure observations from Figure 67(a), there is a trend for forecast

509 temperature overestimation with τ_{550} , on the order of ~ 1 to 2°C . Use of the ECMWF forecast
510 error in the analysis clearly mitigates a significant amount of the non-plume related temperature
511 gradient across the domain. Temperatures in the heavy smoke plume region tended to be over
512 forecasted by 1 to 6°C . Conversely, on either side of the smoke plume, the 30 hr. forecast tends
513 to underestimate temperature by ~ 1 to 2°C , leading to an overall temperature difference of -2 to $-$
514 8°C , only slightly lower than the findings of a similar study by Westphal and Toon (1991). As
515 an example, Grand Forks had a 18:00Z maximum temperature of 23.9°C with a MODIS τ_{550} of
516 4.4, in-comparison to the ECMWF forecast of 26.8°C .

517 We can expand this analysis further, to examine the skill of ECMWF 18:00Z analyses
518 and 542 hour forecasts relative to the 30 hr forecast discussed above. Figure [7a8a-c](#) shows the 0-
519 hr analysis, and 30-hr and 542 -hr forecasts of the 2-m air temperatures from ECMWF. Again,
520 over the Grand Forks region at 18:00 UTC, the actual surface temperature is around 23.9°C . In
521 comparison, the analysis, 30 hr forecast and 542 hr forecasts were 25.2 , 26.8 , and 28.2°C
522 respectively (or ~ 1.3 , 2.9 . and 4.3°C difference). This is not surprising, as (shown later in Table
523 6) a much smaller forecasting error is expected for the 0-hr forecast. Expanding for all data in
524 the domain, figures [7e8d-f](#) show the differences between observed and modeled 2-m air
525 temperatures ($\Delta T_{0\text{hr}}$, $\Delta T_{30\text{hr}}$ and $\Delta T_{542\text{hr}}$) as a function of MODIS τ_{550} . In all cases clear
526 relationships are found. Ultimately, smoke induced cooling for the 542 hr., and 30-hr forecasts
527 and analysis are $-0.9^\circ\text{C}/\tau_{550}$, $-1.0^\circ\text{C}/\tau_{550}$ and $-0.6^\circ\text{C}/\tau_{550}$, respectively. The slope and offset
528 values are also shown in Table 4.

529 The same analysis is also conducted for the analysis, 24-hr and 48-hr forecasts of 1.5-m
530 air temperatures from the UKMO model, and the 0-hr, 24-hr and 48-hr forecasts of 2-m air
531 temperatures from the NCEP model. Similar results, as shown in Figures [78\(a\)-\(f\)](#) for ECMWF,

532 are found and are summarized in Table 4. Similar plots as Figure 7-8 are provided in Appendix
533 Figures ~~A1 and A2(a) and (b)~~ A1 and A2(a) and (b) for UKMO and NCEP respectively. For these other
534 models, smoke induced cooling values range from -0.3 to $-0.8^{\circ}\text{C}/\tau_{550}$ for the analysis, 24- and
535 48-hr forecasts from UKMO and NCEP models. Figure 7-8 and Table 4 suggest that a clear
536 relationship exists between the differences in observed and modeled near surface air temperature
537 (ΔT) and τ_{550} , for the 0-hr, 24(30)-hr and 48(54)-hr forecasts, regardless of the model evaluated.
538 All 9 cases suggest a daytime smoke Aerosol Direct Surface Cooling Efficiency (C_{τ}) on the order
539 of -0.4 to $-0.8^{\circ}\text{C} / \tau_{550}$ (550nm) for 18:00Z analyses, and -0.3 to $-1.0^{\circ}\text{C} / \tau_{550}$ for 24- to 54-hr
540 forecasts, although the slopes could be biased by uncertainties in the numerical simulations.

541 In addition to statistical noise, variability in the daytime smoke C_{τ} could be a function of
542 aerosol properties (e.g., absorption), surface characteristics, and the mixed layer (e.g., stability
543 and advection). From the AERONET data in the region (Table 2), optical properties appear to be
544 consistent over the region. Thus surface or regional attributes are likely a larger source of
545 variability here. We hypothesized that such variability may covary with mean regional surface
546 temperature. In Figure 7-8, the scatter plots of ΔT versus τ_{550} are also plotted as a function of
547 monthly mean temperature at 18:00UTC. To construct the monthly mean temperatures at
548 18:00UTC for each ASOS site, daily observations within ± 10 minutes of 18:00UTC are averaged
549 to represent the daily surface temperature at 18:00UTC. Then, those daily 18:00 UTC values are
550 averaged over the study period of June 15- July 14, 2015, excluding observations from June 29,
551 2015 (Fig. 3-2g). Only ASOS sites having more than 20 daily averages are used. Data pairs with
552 monthly mean temperatures lower than 22°C , between 22 - 24.5°C , and greater than 24.5°C
553 (arbitrarily selected numbers) are colored in blue, green and red, respectively. Data points are
554 largely scattered for the cooler temperatures, representing the far eastern region of the domain.

555 However, steeper slopes are found for middle temperature sites in comparison to those with
556 warmer temperatures. Similar behaviors are also found for all UKMO and NECP model
557 forecasts and analyses (Table 4). This suggests that a higher absolute daytime smoke C_{τ} is
558 expected for areas with monthly mean temperatures of 22-24.5°C in comparison with regions
559 that are typically warmer. Or, a higher absolute daytime smoke C_{τ} is expected for a colder
560 region or a colder season. ~~Considering that the near surface air temperature is modulated by~~
561 ~~radiative warming/cooling and thermal advection, this result may suggest that radiative~~
562 ~~warming/cooling is more dominant for a colder region, which~~ This topic will be further explored
563 in a companion paper.

564

565 **3.4.2 The June 30th case**

566 The second day of the event, June 30th, is less ideal in comparison with the June 29th case,
567 as the smoke plume is less dense, clouds form within the region, and the τ_{550} field has a smaller
568 spatial gradient. Also, the Terra MODIS satellite overpasses are approximate one hour ahead of
569 the model data at 18:00 UTC, and one should expect that both aerosol and temperature fields
570 may change within one hour. However, as an occluded front was moving into the Dakotas, the
571 entire smoke airmass transited fairly uniformly into the upper Mississippi River Valley. Thus it
572 is an interesting analysis to make.

573 Aerosol induced surface cooling, while noisier, is nevertheless observable as shown in
574 Figure [67](#). Figure [67\(d\)](#) shows a Terra MODIS RGB image of the June 30th case over the Upper
575 Mississippi and Ohio Valley region. Similar to June 29th, Figures [6a-7\(a\)](#) and [7\(b\)](#) include the
576 scatter plot of regional T_{obs} and $\Delta T_{30\text{hr}}$ versus Terra MODIS DT τ_{550} . On average, there is a 4°C
577 decrease in observed temperature ~~a 2°C~~ for an increase in MODIS τ_{550} to 4, roughly half the June

578 29th sensitivity. However, the regional temperature gradient with colder temperatures in the
579 great lakes region is even more pronounced (Figure 23(e)), in part leading to this suppressed
580 value. Examining the ECMWF 30 hr forecast, we can draw a similar conclusion, with the model
581 also having low biases in the great lakes region.

582 As shown in Section 3.4.1, similar analyses are conducted for the ECMWF, UKMO and
583 NCEP modeled near-surface air temperatures for the Mississippi and Ohio Valley region, as
584 shown in Table 5. Again, smoke aerosol induced surface cooling is found for all nine scenarios
585 (0, 24-hr and 48-hr forecasts for UKMO and NCEP, 0, 30-hr and 54-hr forecasts for ECMWF).
586 However, smaller daytime smoke C_{τ} values on the order of -0.25 to $-0.5^{\circ}\text{C} / \tau_{550}$ are found for the
587 June 30th case in comparison with the June 29th case. The smaller daytime smoke C_{τ} values may
588 be partially due to a larger temporal difference between the model and satellite data, ~~as well as a~~
589 ~~lower aerosol loading~~ for the June 30th case. But again this may also be a result of a difference in
590 the atmosphere, and atmospheric simulation in the Great Lakes region.

591 Also, as suggested from Section 3.4.1, it is possible that daytime smoke C_{τ} could be a
592 function of surface temperature in itself. Compared to the upper Midwest region, the Mississippi
593 and Ohio River Valley are at lower latitudes with warmer surface temperatures on average, and
594 thus may experience a smaller C_{τ} . To test this hypothesis, monthly mean surface air
595 temperatures at 18:00 UTC are computed from ASOS data, following similar steps mentioned in
596 Section 3.4.1, but with June 30th, 2015 instead of June 29th, 2015 excluded from the monthly
597 averages (Figure 32h). With the constructed monthly mean temperatures for available ASOS
598 stations, the smoke aerosol C_{τ} values are recomputed for all nine scenarios (Table 5), but with
599 the use of only ASOS stations that have monthly mean temperatures lower than 28°C. Lower
600 daytime smoke C_{τ} values on the order of -0.5 to $-1.0^{\circ}\text{C} / \tau_{550}$ are found by restricting the study

601 region to colder areas. Still, these are only potential possibilities for the differences between the
602 June 29th and June 30th cases.

603

604 *3.5 Cooling efficiencies as related to baseline uncertainties for the modeled near surface air* 605 *temperature*

606 The question of how important the smoke cooling efficiency is to numerical weather
607 prediction is fundamentally related to the overall skill of the natural model. Models with large
608 RMSE's will mask the aerosol signal; such models have more important sources of error.
609 Models with high skill, on the other hand, naturally are sensitive to higher order terms. In this
610 section, we examine this phenomenon and by evaluating near-surface air temperature forecasts
611 from ECMWF, UKMO, and NCEP in the Upper Midwest region with respect to smoke τ_{550} for
612 the June 29th case. As the first step, baseline uncertainties in near-surface air temperatures from
613 NCEP, UKMO and ECMWF model runs are evaluated (Table 6) using surface observations from
614 ground stations, as shown in Figure 23(g). To construct Table 6, 0-, 24(30)- and 48(542)-hour
615 (hr.) model forecasts at 18:00UTC from June 15 to July 14 are collocated with ground based
616 ASOS data (the numbers included in parentheses are for ECMWF). The mean and one standard
617 deviation of the differences between forecasted and observed temperatures are computed for the
618 0-, 24(30)- and 48(542)-hr. model forecasts and are represented by ΔT_{0hr} , $\Delta T_{24/30hr}$ and $\Delta T_{48/542hr}$,
619 respectively, in this study. Indicated in Table 6, similar $\Delta T_{48/542hr}$ values of around -1°C with
620 similar one-standard-deviation of $\sim 2.5^{\circ}\text{C}$ are found for the 48-hr forecasted near surface air
621 temperatures from UKMO and NCEP. A smaller $\Delta T_{48/542hr}$ of less than -0.4°C , with a smaller
622 one-standard-deviation of 2.0°C , is found for the 542-hr forecasted 2-m air temperatures from
623 ECMWF. $\Delta T_{24/30hr}$ and one-standard-derivation of $\Delta T_{24/30hr}$ of around -0.8°C and 2.3°C are found

624 for the 24-hr forecasted 2-m air temperatures for NCEP, and the values are -0.6°C and 2.1°C for
625 the 24-hr forecasted 1.5-m air temperatures for UKMO. Again, smaller values of $\Delta T_{24/30hr}$ and
626 one-standard-deviation of -0.2°C and 1.9°C are found for the 30-hr forecasted 2-m air
627 temperatures for ECMWF. In comparison, the 0-hr forecasts of near surface air temperatures
628 exhibit much smaller standard derivations of the differences to the observed surface
629 temperatures; around 1.5°C from all three models.

630 The Root-Mean-Square-Error (RMSE) values for the 0-, 24(30)- and 48(54~~2~~)-hr model
631 forecasted near surface air temperatures are 2.3, 2.5 and 2.7°C for NCEP data, 1.3, 2.2 and 2.7°C
632 for UKMO, and 1.6, 1.9 and 2.0°C for ECMWF model runs, respectively. The same analysis
633 has also been conducted for the June 30th, 2015 case. Not surprisingly, the reported RMSE
634 values are consistent for both the upper Midwest and the Ohio River Valley regions. For
635 example, the computed RMSE values for the June 30th case are 1.5, 2.0, and 2.2 °C for the 0-,
636 30-, and 54-hr ECMWF forecasts. The RMSE values for the 0-, 24-, and 48-hr NECP and
637 UKMO model forecasted near surface air temperatures are 1.9, 2.2, 2.5°C, and 1.3, 2.1, 2.5 °C,
638 respectively.

639 The RMSE values represent the baseline cases for the modeled uncertainty in near
640 surface air temperatures. Theoretically, the effect of aerosols on weather forecasts can likely be
641 detected if the aerosol induced surface cooling is larger than the baseline uncertainties in the
642 modeled near surface air temperatures. Given a rough estimation of $\sim -1.5^\circ\text{C} / \tau_{550}$ for the
643 daytime smoke C_τ , the changes in τ_{550} need to be above ~ 1.5 -2 for the aerosol induced cooling
644 effect to be observable from the 48(54~~2~~)-hr model forecasts. Similarly, τ_{550} values of ~ 1 -1.5 and
645 ~ 1.5 are required for the aerosol induced cooling effect to be detectable from the 0-hr and
646 24(30)-hr model forecasts.

647

648 **4.0 Application: Straw assessment on a global scale**

649 It is suggested from Section 3 that smoke aerosol plumes have a daytime C_{τ} on the order
650 of ~ -0.25 to $-1.5^{\circ}\text{C} / \tau_{550}$. Yet, RMSE values estimated over the study region for the modeled
651 near-surface air temperatures from NCEP, UKMO and ECMWF are on the order of 1.3 - 2.3°C
652 for 0-hr forecasts and are much larger for a longer period of forecasts. Clearly, even with the
653 inclusion of perfect aerosol fields in numerical models, the impact of aerosol particles on near
654 surface temperature forecasts are unlikely to be observable due to the inherent uncertainties in
655 numerical model simulations. An exception to this is a region experiencing very high AOTs, in
656 particular a sharp change in aerosol loading of a significant amount (e.g., daily τ_{550} change > 1
657 for aerosol effects to be observable from 0-hr, near surface air temperature forecasts).

658 Next, we assume the $\sim -1.5^{\circ}\text{C} / \tau_{550}$ daytime C_{τ} is applicable to all aerosol types and the
659 estimated RMSE values from over the study region are applicable on a global scale. Regions
660 whose near-surface air temperature forecasts could potentially be affected by aerosol plumes
661 with a detectable signal are studied. Note that only sharp daily changes in AOT can introduce
662 detectable signals in weather forecasts: for a region with persistent high aerosol loading, the
663 aerosol cooling effects are likely to be accounted for through assimilating meteorological-based
664 observations that are impacted by aerosol particles. As mentioned above, for the aerosol direct
665 cooling effect to be detectable on 0-hr near-surface air temperature forecasts, a minimum sharp
666 daily τ_{550} change of approximately 1 is required. Therefore, using one year of Collection 6
667 MODIS Dark Target (DT) and Deep Blue (DB) aerosol products from both Aqua and Terra, we
668 have studied regions that have sharp daily AOT changes above 1.

669 For illustration purposes, Figures 89(a) and 89(b) show the spatial distribution of yearly
670 mean MODIS AOT and the number of days with MODIS τ_{550} larger than 1, respectively, at a
671 spatial resolution of 0.5 degree (Latitude/Longitude), constructed using C6 Aqua and Terra
672 aerosol products for 2014. The combined DT and DB data, which are included in C6 MODIS
673 aerosol products, are used. Also, “bad” retrievals, as indicated by the QA flag included in the
674 products, are discarded.

675 The global yearly average τ_{550} , as shown in Figure 89(a), is consistent with the spatial
676 τ_{550} distributions as reported from previous studies (e.g. Levy et al., 2013; Zhang and Reid,
677 2010). Also, not surprisingly, regions with MODIS τ_{550} larger than 1 (Figure 89(b)), which
678 include Central and North Africa, Middle East, India, Eastern Asia, South-East Asia and Upper
679 North America. In particular, over India and East China, the number of τ_{550} -larger-than-1 days
680 exceeds 2 months, indicating potential severe aerosol pollution issues for the two regions.

681 Using the MODIS aerosol products as shown in Figures 89p(a) and (b), the 0.5°
682 (Latitude/Longitude) gridded daily AOT data from a given day are compared with the gridded
683 daily AOT data from the next day. If a change in τ_{550} of larger than 1.0 is found for a 0.5°
684 (Latitude/Longitude) grid box, the event is recorded. Figure 89p(c) shows the global
685 distribution of the number of cases when sharp changes of τ_{550} of > 1 are detected for a 0.5°
686 (Latitude/Longitude) grid box. A total of one year (2014) of Terra and Aqua combined DT and
687 DB τ_{550} data are used. However, the average number of cases with sharp τ_{550} changes are rather
688 low in general, indicating that even by incorporating an accurate aerosol field in a numerical
689 model, the aerosol induced surface cooling effect would remain mostly undetected for the 0-hr
690 forecast due to relatively larger uncertainties in modeled near-surface air temperatures. Still,
691 Figure 89p(c) suggests that for regions such as East China, East Russia, India and portions of the

692 Saharan and Taklimakan Deserts, sharp changes in τ_{550} of above 1 happen more than 10 times a
693 year. These are the regions where incorporating aerosol models is likely to have the most impact
694 on weather forecasts of near-surface air temperatures.

695 Lastly, readers should be aware that aerosol plumes with extreme high aerosol loadings
696 could be misidentified as clouds, thus these aerosol plumes could be excluded from the MODIS
697 DT/DB retrievals (e.g. Alfaro-Contreras et al., 2015). Therefore, the frequency distribution of
698 the sharp aerosol loading changes, as shown in Figure 89(c), is likely underestimated. Still, this
699 is the first attempt at such efforts, and is worth reporting.

700

701 5 Conclusions and Implications

702 In this study, the effect of smoke aerosol plumes on 2-m (1.5-m for the UKMO model) air
703 temperature forecasts from European Center for Medium range Weather Forecasting (ECMWF),
704 National Centers for Environmental Prediction (NCEP), United Kingdom Meteorological Office
705 (UKMO) models are investigated over a significant smoke aerosol event that happened on June
706 28th - June 30th, 2015 over the Midwestern US. The smoke aerosol induced daytime direct
707 surface cooling effect is studied and the baseline uncertainties in the modeled near surface air
708 temperatures are evaluated over the study domain. This study suggests:

709 (1) Consistent with several previous studies, the June 29th, 2015 smoke event introduced a
710 noticeable surface cooling of $\sim 5^{\circ}\text{C}$ over Grand Forks, ND. The smoke aerosol induced
711 daytime direct surface cooling efficiency (C_{τ}) is estimated to be $\sim -1.5^{\circ}\text{C}$ per 1.0 AOT
712 (550nm, τ_{550}).

713 (2) The differences in modeled 2-m/1.5-m air temperatures from NCEP, UKMO and
714 ECMWF models and observed near surface air temperatures (ΔT) are studied as a

715 function of MODIS τ_{550} for 0-, 24-, and 48-hr forecasts (0-, 30-, and 542-hr forecasts for
716 the ECMWF model) for the June 29th, 2015 smoke event. All nine cases show a clear
717 decrease in ΔT as τ_{550} increases to 4, indicating that smoke event does have an observable
718 cooling effect on the near surface air temperature forecasts, with an estimated daytime C_{τ}
719 on the order of -0.5°C to -1°C per unit τ_{550} . Still, those C_{τ} values are likely to be affected
720 by uncertainties in modeled temperatures.

721 (3) Similar analysis was also conducted on June 30th, 2015 over the Ohio River Valley.
722 Again, the smoke aerosol plume induced surface cooling is found from all nine scenarios,
723 however with a smaller (in magnitude) daytime C_{τ} on the order of -0.25°C to -0.5°C per
724 unit τ_{550} . Further analysis seems to indicate that C_{τ} may also be a function of surface
725 temperature, and a smaller (in magnitude) daytime C_{τ} may be expected over a warmer
726 region. This hypothesis will be further examined in a modeling-based paper.

727 (4) Using one month of observed surface temperatures from the study region, baseline
728 uncertainties for near surface air temperatures from the 0-, 24(30)-, and 48(542)-hr
729 forecasts are estimated to be 1.3-2.3, 2.0-2.5 and 2.0-2.7 $^{\circ}\text{C}$, respectively. Thus, for the
730 aerosol induced direct cooling effect to be observable from the 0-hr model forecasted
731 near surface air temperature fields, a daily change in τ_{550} of ~ 1.0 - 1.5 (550nm) is needed.
732 Similar requirements in τ_{550} of ~ 1.5 and ~ 1.5 - 2.0 are needed for the aerosol direct cooling
733 effect to be detected from 24(30)-hr. and 48(542)-hr. forecasted near surface air
734 temperature fields respectively, assuming the estimated daytime C_{τ} of $\sim -1.5^{\circ}\text{C}$ per unit
735 τ_{550} is applicable to all cases.

736 (5) Using one year of Terra and Aqua Collection 6 MODIS combined Dark Target and Deep
737 Blue aerosol products, the number of days with significant changes in daily τ_{550} of >1 are

738 estimated. Globally, events with a daily τ_{550} change of >1 are rare, indicating that at the
739 current stage, incorporating aerosol models in-line with a weather forecasting model is
740 unlikely to introduce a noticeable improvement in the forecasted near surface air
741 temperatures. Still, for regions such as Eastern China, Eastern Russia, India and portions
742 of Saharan and Taklimakan deserts, the number of days with sharp τ_{550} changes are above
743 10 for the year 2014, showing that accurate aerosol analysis may be needed for weather
744 forecasts for these regions.

745 ~~(5)~~(6) Note that this study is focused on cloud free conditions and only the direct smoke
746 aerosol surface cooling effect is studied. Still, aerosol particles may indirectly affect
747 weather by altering cloud microphysics in both strati-form and convective clouds (e.g.
748 Tao et al., 2012). Such effects warrant further discussions and evaluations.

Formatted: Font: (Default) Times New Roman, 12 pt

749 Through an observational-based analysis, this study suggests that aerosol particles do have an
750 observable cooling effect on near surface air temperatures. In a companion paper, the aerosol
751 induced direct cooling effect will be further explored from a modeling perspective with the use
752 of a numerical model in-line with an aerosol transport model. Lastly, we expect, with the
753 improvement in accuracy of numerical forecasting models in the future, the inclusion of accurate
754 aerosol estimates will be unavoidable for the further improvement of numerical weather
755 forecasts.

756

757

758 **Acknowledgments:**

759 Authors JZ and MC acknowledge the support of the NASA project NNX14AJ13G and the NSF
760 project IIA-1355466. Author JSR was supported by ONR Code 322 (N0001415WX00854). We

761 thank the THORPEX Interactive Grand Global Ensemble (TIGGE) group for the NCEP and UK
762 Met office model data. We thank the Iowa Environmental Mesonet (IEM) for surface-based
763 meteorological observations. We also thank AERONET program and their affiliated members
764 for the surface-based aerosol optical property measurements. Editorial support from E. A. Reid
765 is gratefully acknowledged.

766

767 **References**

- 768 Adhikary, Kulkarni B., S., Dallura A., Tang Y., Chai T., Leung L. R., Qian Y., Chung C. E.,
769 Ramanathan V., and Carmichael G. R.: A regional scale chemical transport modeling of
770 Asian aerosols with data assimilation of AOD observations using optimal interpolation
771 technique, *Atmos. Environ.*, 42(37), 8600–8615, 2008.
- 772 Alfaro-Contreras, R., Zhang, J., Campbell, J. R., and Reid, J. S.: Investigating the frequency and
773 trends in global above-cloud aerosol characteristics with CALIOP and OMI, *Atmos.*
774 *Chem. Phys. Discuss.*, 15, 4173-4217, doi:10.5194/acpd-15-4173-2015, 2015.
- 775 Benedetti, A., et al.: Aerosol analysis and forecast in the European Centre for Medium-Range
776 Weather Forecasts Integrated Forecast System: 2. Data assimilation, *J. Geophys. Res.*,
777 114, D13205, doi:10.1029/2008JD011115, 2009.
- 778 Bougeault P., Toth Z., Bishop C., Brown B., Burridge D., Chen D. H., Ebert B., Fuentes M.,
779 Hamill T. M., Mylne K., Nicolau J., Paccagnella T., Park Y.-Y., Parsons D., Raoult B.,
780 Schuster D., Silva Dias P., Swinbank R., Takeuchi Y., Tennant W., Wilson L., Worley
781 S.: The THORPEX interactive grand global ensemble. *Bull. Am. Meteorol. Soc.* 91:
782 1059–1072, 2010.
- 783 Chapman, E. G., Gustafson Jr., W. I., Easter, R. C., Barnard, J. C., Ghan, S. J., Pekour, M. S.,
784 and Fast, J. D.: Coupling aerosol-cloud-radiative processes in the WRF-Chem model:
785 Investigating the radiative impact of elevated point sources, *Atmos. Chem. Phys.*, 9, 945-
786 964, doi:10.5194/acp-9-945-2009, 2009.
- 787 Chew, B. N., Campbell, J. R., Reid, J. S., Giles, D. M., Welton, E. J., Salinas S. V., and Liew S.
788 C: Tropical cirrus cloud contamination in sun photometer data, *Atmos. Environ.*, *Atmos.*
789 *Env.*, 45, 6724-6731, doi:10.1016/j.atmosenv.2011.08.017, 2011.

790 Colarco, P. R., Schoeberl, M. R., Doddridge, B. G., Marufu, L. T., Torres, O. and Welton E. J.
791 2004: Transport of smoke from Canadian forest fires to the surface near Washington,
792 D.C.: Injection height, entrainment, and optical properties, *J. Geophys. Res.*, 109,
793 D06203, doi:[10.1029/2003JD004248](https://doi.org/10.1029/2003JD004248), 2014.

794 Colarco, P., da Silva, A., Chin, M., and Diehl, T.: Online simulations of global aerosol
795 distributions in the NASA GEOS-4 model and comparisons to satellite and ground-based
796 aerosol optical depth, *J. Geophys. Res.*, 115, D14207, doi:10.1029/2009JD012820, 2010.

797 Collins, W. D., Rasch P. J., Eaton B. E., Khattatov B. V., Lamarque J.-F., and Zender C. S.:
798 Simulating aerosols using a chemical transport model with assimilation of satellite
799 aerosol retrievals: Methodology for INDOEX, *J. Geophys. Res.*, 106(D7), 7313–7336,
800 doi:[10.1029/2000JD900507](https://doi.org/10.1029/2000JD900507), 2001.

801 Cook, J. and Highwood, E. J.: Climate response to tropospheric absorbing aerosols in an
802 intermediate general-circulation model. *Q.J.R. Meteorol. Soc.*, 130: 175–191.
803 doi: 10.1256/qj.03.64, 2004.

804 Dee, D. P., et al.: The ERA-Interim reanalysis: Configuration and performance of the data
805 assimilation system. *Quart. J. R. Meteorol. Soc.*, 137, 553-597. DOI: 10.1002/qj.8, 2011.

806 Draxler, R. R., and Hess G. D.: Description of the HYSPLIT_4 modeling system. NOAA Tech.
807 Memo. ERL ARL-224, NOAA Air Resources Laboratory, Silver Spring, MD, 24 pp,
808 1997

809 Dubovik, O., and King M. D.: , A flexible inversion algorithm for the retrieval of aerosol optical
810 properties from Sun and sky radiance measurements, *J. Geophys. Res.*, 105, 20,673–
811 20,696, doi:10.1029/ 2000JD900282, 2000.

812 Ge, C., Wang, J., and Reid J. S.: Mesoscale modeling of smoke transport over the Southeast
813 Asian Maritime Continent: coupling of smoke direct radiative feedbacks below and
814 above the low-level clouds, *Atmos. Chem. Phys.*, 14, 159-174, doi:10.5194/acp-14-159-
815 2014, 2014.

816 Generoso, S., Bréon F.-M., Chevallier F., Balkanski Y., Schulz M., and Bey I.: Assimilation of
817 POLDER aerosol optical thickness into the LMDz-INCA model: Implications for the
818 Arctic aerosol burden, *J. Geophys. Res.*, 112, D02311, doi:10.1029/2005JD006954,
819 2007.

820 Grell, G., Freitas, S. R., Stuefer, M., and Fast, J.: Inclusion of biomass burning in WRF-Chem:
821 impact of wildfires on weather forecasts, *Atmos. Chem. Phys.*, 11, 5289-5303,
822 doi:10.5194/acp-11-5289-2011, 2011.

823 Holben, B. N., Eck T. F., Slutsker I., Tanré D., Buis J. P., Setzer A., Vermote E., Reagan J. A.,
824 Kaufman Y. J., Nakajima T., Lavenu F., Jankowiak I., and Smirnov A.: AERONET - A
825 Federated Instrument Network and Data Archive for Aerosol Characterization, *Rem.
826 Sens. Environ.*, 66, 1-16, 1998.

827 Hsu, N. C., Jeong M.-J., Bettenhausen C., Sayer A. M., Hansell R., Seftor C. S., Huang J., and
828 Tsay S.-C.: Enhanced Deep Blue aerosol retrieval algorithm: The second generation, *J.
829 Geophys. Res. Atmos.*, 118, doi:10.1002/jgrd.50712, 2013.

830 Intergovernmental Panel on Climate Change Working Group I Contribution to the IPCC Fifth
831 Assessment Report Climate Change 2013: The Physical Science Basis. Geneva: IPCC.
832 <http://www.ipcc.ch/report/ar5/wg1/#.UqgAXQSiSo>, 2013.

833 Jacobson, M. Z.: Effects of biomass burning on climate, accounting for heat and moisture fluxes,
834 black and brown carbon, and cloud absorption effects, *J. Geophys. Res.*
835 *Atmos.*, 119, 8980–9002, doi:[10.1002/2014JD021861](https://doi.org/10.1002/2014JD021861), 2014

836 Jacobson, M. Z., and Kaufman Y. J.: Wind reduction by aerosol particles, *Geophys. Res.*
837 *Let.*, 33, L24814, doi:[10.1029/2006GL027838](https://doi.org/10.1029/2006GL027838), 2006.

838 Justice, C.O., Giglio, L., Korontzi, S., Owens, J., Morisette, J.T., Roy, D., Descloitres, J.,
839 Alleaume, S., Petitcolin, F., Kaufman, Y. J.: The MODIS fire products. *Remote Sens.*
840 *Environ.* 83, 244–262, 2002.

841 Lau, K.-M., and Kim K.-M.: Observational relationships between aerosol and Asian monsoon
842 rainfall, and circulation, *Geophys. Res. Lett.*, 33, L21810, doi:[10.1029/2006GL027546](https://doi.org/10.1029/2006GL027546),
843 2006.

844 Kahn, R. A., Gaitley B. J., Garay M. J., Diner D. J., Eck T. F., Smirnov A., and Holben B. N.:
845 Multiangle Imaging SpectroRadiometer global aerosol product assessment by comparison
846 with the Aerosol Robotic Network, *J. Geophys. Res.*, 115, D23209,
847 doi:[10.1029/2010JD014601](https://doi.org/10.1029/2010JD014601), 2010.

848 Kahnert, M.: Variational data analysis of aerosol species in a regional CTM: background error
849 covariance constraint and aerosol optical observation operators. *Tellus B*, 60: 753–770.
850 doi: 10.1111/j.1600-0889.2008.00377.x, 2008.

851 Kaku, K. C., Reid, J. S., O'Neill, N. T., Quinn, P. K., Coffman, D. J., and Eck, T. F.: Verification
852 and application of the extended spectral deconvolution algorithm (SDA+) methodology
853 to estimate aerosol fine and coarse mode extinction coefficients in the marine boundary
854 layer, *Atmos. Meas. Tech.*, 7, 3399–3412, doi:10.5194/amt-7-3399-2014, 2014.

855 Kolusu, S. R., Marsham, J. H., Mulcahy, J., Johnson, B., Dunning, C., Bush, M., and
856 Spracklen, D. V.: Impacts of Amazonia biomass burning aerosols assessed from short-
857 range weather forecasts, *Atmos. Chem. Phys.*, 15, 12251-12266, doi:10.5194/acp-15-
858 12251-2015, 2015.

859 Kukkonen, J., Olsson, T., Schultz, D. M., Baklanov, A., Klein, T., Miranda, A. I., Monteiro, A.,
860 Hirtl, M., Tarvainen, V., Boy, M., Peuch, V.-H., Poupkou, A., Kioutsioukis, I., Finardi,
861 S., Sofiev, M., Sokhi, R., Lehtinen, K. E. J., Karatzas, K., San José, R., Astitha, M.,
862 Kallos, G., Schaap, M., Reimer, E., Jakobs, H., and Eben, K.: A review of operational,
863 regional-scale, chemical weather forecasting models in Europe, *Atmos. Chem. Phys.*, 12,
864 1–87, doi:10.5194/acp-12-1-2012, 2012.

865 Levy, R. C., Mattoo, S., Munchak, L. A., Remer, L. A., Sayer, A. M., Patadia, F., and Hsu, N.
866 C.: The Collection 6 MODIS aerosol products over land and ocean, *Atmos. Meas. Tech.*,
867 6, 2989–3034, doi:10.5194/amt-6-2989-2013, 2013.

868 Lin, C., Wang Z., and Zhu J.: An ensemble Kalman filter for severe dust storm data assimilation
869 over China, *Atmos. Chem. Phys.*, 8, 2975-2983, doi:10.5194/acp-8-2975-2008, 2008.

870 Mulcahy, J. P., Walters, D. N., Bellouin, N., and Milton, S. F.: Impacts of increasing the aerosol
871 complexity in the Met Office global numerical weather prediction model, *Atmos. Chem.*
872 *Phys.*, 14, 4749-4778, doi:10.5194/acp-14-4749-2014, 2014.

873 Niu, T., Gong S. L., Zhu G. F., Liu H. L., Hu X. Q., Zhou C. H., and Wang Y. Q.: Data
874 assimilation of dust aerosol observations for the CUACE/dust forecasting system, *Atmos.*
875 *Chem. Phys.*, 8, 3473-3482, doi:10.5194/acp-8-3473-2008, 2008.

876 O’Neill, N. T., Campanelli M., Lupu A., Thulasiraman S., Reid J. S., Aube M., Neary L.,
877 Kaminski J. W., and McConnel J. C.: Evaluation of the GEM-AQ air quality model

878 during the Quebec smoke event of 2002: Analysis of extensive and intensive optical
879 disparities, *Atmos. Environ.*, 40, 3737-3749, 2005.

880 O'Neill, N. T., Eck T. F., Smirnov A., Holben B. N., and Thulasiraman S.: Spectral
881 discrimination of coarse and fine mode optical depth, *J. Geophys. Res.*, 108(D17), 4559,
882 doi:10.1029/2002JD002975, 2003.

883 Pagowski, M., and Grell G. A.: Experiments with the assimilation of fine aerosols using an
884 ensemble Kalman filter, *J. Geophys. Res.-Atmos.*, 117, D21302,
885 doi:10.1029/2012jd018333, 2012.

886 Pérez, C., Nickovic S., Pejanovic G., Baldasano J. M., and Özsoy E.: Interactive dust-
887 radiation modeling: A step to improve weather forecasts, *J. Geophys. Res.*, 111, D16206,
888 doi:[10.1029/2005JD006717](https://doi.org/10.1029/2005JD006717), 2006. Pérez, C., Hausteijn, K., Janjic, Z., Jorba, O., Huneeus,
889 N., Baldasano, J. M., Black, T., Basart, S., Nickovic, S., Miller, R. L., Perlwitz, J. P.,
890 Schulz, M., and Thomson, M.: Atmospheric dust modeling from meso to global scales
891 with the online NMMB/BSC-Dust model – Part I: Model description, annual simulations
892 and evaluation, *Atmos. Chem. Phys.*, 11, 13001– 13027, doi:10.5194/acp-11-13001-
893 2011, 2011.

894 Reid, J. S., Eck T., Christopher S., Dubovik O., Koppmann R., Eleuterio D., Holben B., Reid E.,
895 and Zhang J.: A review of biomass burning emissions part III: Intensive optical properties
896 of biomass burning particles, *Atmos. Chem. Phys.*, 5, 827–849, SRef-ID: 1680-
897 7324/acp/2005-5-827. <http://www.atmos-chem-phys.org/acp/5/827/>, 2005.

898 Remy, S., Benedetti A., Bozzo A., Haiden T., Jones L., Razinger M., Flemming J., Engelen R. J.,
899 Peuch V. H., and Theaut J. N.: Feedbacks of dust and boundary layer meteorology during
900 a dust storm in the eastern Mediterranean, *Atmos. Chem. And Phys.* In press, 2015.

901 Robock, A., Surface cooling due to forest fire smoke, *J. Geophys. Res.*, 96(D11), 20869–20878,
902 doi:[10.1029/91JD02043](https://doi.org/10.1029/91JD02043), 1991.

903 Rubin, J. I., Reid J. S., Hansen J. A., Anderson J. L., Collins N., Hoar T. J., Hogan T., Lynch
904 P., McLay J., Reynolds C. A., Sessions W. R., Westphal D. L., and Zhang J.:
905 Development of the Ensemble Navy Aerosol Analysis Prediction System (ENAAPS) and
906 its application of the Data Assimilation Research Testbed (DART) in support of aerosol
907 forecasting, *Atmos. Chem. Phys. Discuss.*, 15, 28069-28132, doi:10.5194/acpd-15-
908 28069-2015, 2015.

909 Schutgens, N. A. Miyoshi J., T., Takemura T., and Nakajima T.: Applying an ensemble Kalman
910 filter to the assimilation of AERONET observations in a global aerosol transport model,
911 *Atmos. Chem. Phys.*, 10, 2561-2576, 2010.

912 Sessions, W. R., Reid, J. S., Benedetti, A., Colarco, P. R., da Silva, A., Lu, S., Sekiyama, T.,
913 Tanaka, T. Y., Baldasano, J. M., Basart, S., Brooks, M. E., Eck, T. F., Iredell, M.,
914 Hansen, J. A., Jorba, O. C., Juang, H.-M. H., Lynch, P., Morcrette, J.-J., Moorthi, S.,
915 Mulcahy, J., Pradhan, Y., Razinger, M., Sampson, C. B., Wang, J., and Westphal, D. L.:
916 Development towards a global operational aerosol consensus: basic climatological
917 characteristics of the International Cooperative for Aerosol Prediction Multi-Model
918 Ensemble (ICAP-MME), *Atmos. Chem. Phys.*, 15, 335-362, doi:10.5194/acp-15-335-
919 2015, 2015.

920 Shi, Y., Zhang, J., Reid, J. S., Holben, B., Hyer, E. J., and Curtis, C., An analysis of the
921 collection 5 MODIS over-ocean aerosol optical depth product for its implication in
922 aerosol assimilation, *Atmos. Chem. Phys.*, 11, 557–565, doi:10.5194/acp-11-557-2011,

923 2011. Tanaka, T. Y. and Chiba, M.: Global simulation of dust aerosol with a chemical
924 transport model, *MASINGAR, J. Meteorol. Soc. Jpn.*, 83, 255–278, 2005.

925 Tesfaye, M., Tsidu G. M., Botai J., Sivakumar V., and Rautenbach C. J. D.: Mineral dust aerosol
926 distributions, its direct and semi-direct effects over South Africa based in regional
927 climate model simulations, *J. of Arid Environ.*, 114, 22-40, 2015

928 Tombette, M., Chazette, P., Sportisse, B., and Roustan, Y.: Simulation of aerosol optical
929 properties over Europe with a 3-D size-resolved aerosol model: comparisons with
930 AERONET data, *Atmos. Chem. Phys.*, 8, 7115–7132, doi:10.5194/acp-8-7115-2008,
931 2008.

932 Westphal, D. L., and Toon O. B.: Simulations of microphysical, radiative, and dynamical
933 processes in a continental-scale forest fire smoke plume, *J. Geophys. Res.*, 96(D12),
934 22379–22400, doi:[10.1029/91JD01956](https://doi.org/10.1029/91JD01956), 1991.

935 Yu, H., Dickinson R. E., Chin M., Kaufman Y. J., Holben B. N., Geogdzhayev I. V., and
936 Mishchenko M. I.: Annual cycle of global distributions of aerosol optical depth from
937 integration of MODIS retrievals and GOCART model simulations, *J. Geophys. Res.*, 108,
938 4128, doi:[10.1029/2002JD002717](https://doi.org/10.1029/2002JD002717), D3, 2003.

939 Zhang, J. Reid, J. S., Westphal, D. L., Baker, N. L., and Hyer, E. J.: A system for operational
940 aerosol optical depth data assimilation over global oceans, *J. Geophys. Res.*, 113,
941 D10208, doi:10.1029/2007JD009065, 2008.

942 Zhang, J. and Reid, J. S.: A decadal regional and global trend analysis of the aerosol optical
943 depth using a data-assimilation grade over-water MODIS and Level 2 MISR aerosol
944 products, *Atmos. Chem. Phys. Discuss.*, 10, 18879-18917, doi:10.5194/acpd-10-18879-
945 2010, 2010.

946 Zhang, J., Campbell, J. R., Reid, J. S., Westphal, D. L., Baker, N. L., Campbell, W. F., and Hyer,
947 E. J.: Evaluating the impact of assimilating CALIOP-derived aerosol extinction profiles
948 on a global mass transport model, *Geophys. Res. Lett.*, 38, L14801,
949 doi:10.1029/2011GL047737, 2011.

950 Zhang J., Reid J. S., Campbell J. R., Hyer E. J., and Westphal D. L.: Evaluating the Impact of
951 Multi-Sensor Data Assimilation on A Global Aerosol Particle Transport Model. *J.*
952 *Geophys. Res. Atmos.*, 119, 4674–4689, doi:[10.1002/2013JD020975](https://doi.org/10.1002/2013JD020975), 2014.

953

954

955

956 **Table Captions**

957 **Table 1** – Missing data for the NCEP model runs (Data are not available from the TIGGE site).

958
959 **Table 2** – Averaged aerosol-related-properties, including effective radius (r_{eff}), up-welling and
960 down-welling aerosol forcing efficiencies (at 550nm), and Single Scattering Albedo (SSA),
961 ~~corresponding to Dubovik as~~ retrievals~~ed~~ from measurements from 4 selected AERONET
962 stations for June 29-July 3, 2015.

963
964 **Table 3** – The monthly mean differences (ΔT) as well as correlations in the observed daily
965 maximum temperatures between Grand Forks, ND (GFK) and three ASOS site: Bismarck, ND
966 (west of GFK), Roseau and Baudette, MN (east of GFK) for June 15-July 14, 2015, excluding
967 June 29, 2015. The daily maximum temperature differences (ΔT) in between GFK and other
968 three ASOS sites on June 29, 2015 are also reported. Also included are the latitude, longitude of
969 the three ASOS sites and the MODIS reported τ_{550} values (17:47UTC, 550nm).

970
971 **Table 4** – Offsets ($^{\circ}\text{C}$) and slopes ($^{\circ}\text{C}/\tau_{550}$) of MODIS AOT (550nm) versus the differences
972 between observed (using ground stations as shown in Figure ~~6e7(c)~~) and modeled near surface
973 air temperatures (at 18:00UTC, June 29, 2015) from ECMWF, UKMO and NCEP model runs.
974 Similar results using only stations with monthly mean temperatures (\bar{T}) within the range of 22
975 $^{\circ}\text{C}$ to 24.5 $^{\circ}\text{C}$, as well as for stations with $\bar{T} > 24.5$ $^{\circ}\text{C}$ are also shown.

976
977 **Table 5** – Offsets ($^{\circ}\text{C}$) and slopes ($^{\circ}\text{C}/\tau_{550}$) of MODIS τ_{550} (550 nm) versus the differences
978 between observed (using ground stations as shown in Figure ~~7e6(d)~~) and modeled near surface air
979 temperatures (at 18:00UTC, June 30, 2015) from ECMWF, UKMO and NCEP model runs.
980 Similar results are also shown for using only stations with monthly mean temperatures (\bar{T}) less
981 than 28 $^{\circ}\text{C}$.

982
983 **Table 6** – The means and one standard deviations of the differences in observed and modeled
984 near surface air temperatures ($T_{\text{ground-FC}}$) for 0-, 24-, and 48-hour (0-, 30- and ~~542~~-hour for
985 ECMWF) forecasts for NCEP, UKMO and ECMWF model runs over the upper Midwest region.
986 The modeled data are compared with surface temperature measurements from ground stations as
987 shown in Figure ~~2a-3(a)~~ for the period of June 15 –July 14, 2015 (excluding June 29, 2015 data).

988

989

990

991

992

993

994

995 **Table 1** – Missing data for the NCEP model runs (Data are not available from the TIGGE site).

| NCEP | Missing data | 996 |
|-------------------------|-----------------------------|------|
| 0-hour forecast | June 20, 22, 25, July 5, 14 | 997 |
| 24-hour forecast | June 21, 23, 26, July 6 | 998 |
| 48-hour forecast | June 22, 24, 27, July 7 | 999 |
| | | 1000 |

1001

1002

1003 **Table 2** – Averaged aerosol-related-properties, including effective radius (r_{eff}), up-welling and
 1004 down-welling aerosol forcing efficiencies (at 500nm), and Single Scattering Albedo (SSA), ~~as~~
 1005 [corresponding to Dubovik retrieval](#) ~~see~~ from measurements from 4 selected AERONET stations
 1006 for June 29-July 3, 2015.

| | Grand Forks | Sioux City Falls | Ames | Bondville |
|--|---------------------------|-----------------------------|----------------------------|---------------------------|
| N | 7 | 7 | 11 | 5 |
| AOT (500 nm) | 1.4+/-0.6 | 1.3+/-0.16 | 0.5+/-0.12 | 0.8+/-0.4 |
| r_{eff} (μm) | 0.162+/-0.017 -50+/-5 | 0.164+/-0.017 -48+/-12 | 0.160+/-0.012 -55+/-10 | 0.170+/-0.013 -58+/-9 |
| Up. Forcing Eff. ($\text{W m}^{-2} \tau_{500}^{-1}$) | -118+/-16 | -122+/-15 | -165+/-27 | -124+/-10 |
| Down Forcing Eff. ($\text{W m}^{-2} \tau_{500}^{-1}$) | 0.94+/-0.01 | 0.94+/-0.01 | 0.93+/-0.01 | 0.95+/-0.01 |
| SSA(440 nm) | | | | |
| SSA(670 nm) | 0.94+/-0.02 | 0.93+/-0.02 | 0.91+/-0.02 | 0.945+/-0.015 |
| SSA(870 nm) | 0.93+/-0.03 | 0.92+/-0.03 | 0.88+/-0.02 | 0.94+/-0.01 |
| SSA(1020 nm) | 0.92+/-0.03 | 0.92+/-0.03 | 0.86+/-0.03 | 0.93+/-0.01 |

1007
 1008
 1009
 1010

Table 3 – The monthly mean differences (ΔT) as well as correlations in the observed daily maximum temperatures between Grand Forks, ND (GFK) and three ASOS site: Bismarck, ND (west of GFK), Roseau and Baudette, MN (east of GFK) for June 15-July 14, 2015, excluding June 29, 2015. The daily maximum temperature differences (ΔT) in between GFK and other three ASOS sites on June 29, 2015 are also reported. Also included are the latitude, longitude of the three ASOS sites and estimated τ_{550} values from MODIS (17:47UTC, 550nm).

| Location | Relative to the GFK site | Lat. (°) | Long. (°) | R ² | MODIS τ_{550} 17:47Z | Mean ΔT (° C) | ΔT (° C) (June 29) |
|--------------|--------------------------|----------|-----------|----------------|---------------------------|-----------------------|----------------------------|
| Bismarck, ND | West | 46.8 | -100.8 | 0.81 | 0.35 | -1.0 ± 2.0 | -7.8 |
| Roseau, MN | East | 48.8 | -95.7 | 0.55 | 0.84 | 2.5 ± 2.7 | -0.6 |
| Baudette, MN | East | 48.7 | -94.6 | 0.56 | 1.06 | 2.4 ± 2.7 | 1.1 |

Table 4 – Offsets (°C) and slopes (°C/ τ_{550}) of MODIS τ_{550} versus the differences between observed (using ground stations as shown in Figure 76c) and modeled near surface air temperatures (at 18:00UTC, June 29, 2015) from ECMWF, UKMO and NCEP model runs. Similar results using only stations with monthly mean temperatures (\bar{T}) within the range of 22 °C to 24.5°C, as well as for stations with $\bar{T} > 24.5$ °C are also shown.

| Offset / Slope | ECMWF | UKMO | NCEP |
|-------------------------------|----------------------------|----------------------------|----------------------------|
| | (°C) / (°C/ τ_{550}) | (°C) / (°C/ τ_{550}) | (°C) / (°C/ τ_{550}) |
| 0-hour forecast | 0.70/-0.56 | 0.15/-0.38 | -0.39/-0.81 |
| (22 °C < \bar{T} < 24.5 °C) | (1.03/-0.72) | (0.22/-0.46) | (-0.47/-0.86) |
| (\bar{T} > 24.5 °C) | (0.17/-0.27) | (0.06/-0.14) | (-0.31/-0.45) |
| 24 (30)-hour forecast | 1.08/-1.02 | -0.40/-0.71 | 0.62/-0.55 |
| (22 °C < \bar{T} < 24.5 °C) | (1.49/-1.18) | (0.51/-1.01) | (-0.83/-0.68) |
| (\bar{T} > 24.5 °C) | (0.77/-0.71) | (-0.92/-0.36) | (0.93/-0.16) |
| 48 (54)-hour forecast | 0.96/-0.93 | 0.03/-0.67 | 0.18/-0.31 |
| (22 °C < \bar{T} < 24.5 °C) | (1.44/-1.13) | (0.75/-0.88) | (0.72/-0.52) |
| (\bar{T} > 24.5 °C) | (0.48/-0.50) | (-0.37/-0.54) | (0.31/0.04) |

Table 5 – Offsets (°C) and slopes (°C/ τ_{550}) of MODIS τ_{550} versus the differences between observed (using ground stations as shown in Figure 76d) and modeled near surface air temperatures (at 18:00UTC, June 30, 2015) from ECMWF, UKMO and NCEP model runs. Similar results for stations with monthly mean temperatures (\bar{T}) less than 28 °C are also shown.

| Offset / Slope | ECMWF | UKMO | NCEP |
|-----------------------------|----------------------------|----------------------------|----------------------------|
| | (°C) / (°C/ τ_{550}) | (°C) / (°C/ τ_{550}) | (°C) / (°C/ τ_{550}) |
| 0-hour forecast | -0.01/-0.29 | -0.59/-0.17 | 0.08/-0.25 |
| ($\bar{T} < 28$ °C) | (0.24/-0.41) | (0.27/-0.43) | (-0.14/-0.33) |
| 24(30)-hour forecast | 0.18/-0.52 | 0.78/-0.42 | -1.27/-0.30 |
| ($\bar{T} < 28$ °C) | (1.76/-1.05) | (-0.57/-0.57) | (1.61/-0.62) |
| 48(54)-hour forecast | 0.17/-0.20 | 1.20/-0.44 | -1.46/-0.29 |
| ($\bar{T} < 28$ °C) | (1.70/-0.63) | (-0.94/-0.59) | (1.67/-0.50) |

Table 6 – The means and one-standard-deviations (1-STD) of the differences in observed and modeled near surface air temperatures ($T_{\text{ground-FC}}$) for 0-, 24-, and 48-hour (0-, 30- and ~~54~~-hour for ECMWF) forecasts for NCEP, UKMO and ECMWF model runs over the upper Midwest region. The modeled data are compared with surface temperature measurements from ground stations as shown in Figure [32\(a\)](#) for the period of June 15 –July 14, 2015 (excluding June 29, 2015 data).

| | ECMWF (°C) | | | UKMO (°C) | | | NCEP (°C) | | |
|------------------------|---------------|-------|-------|--------------|-------|-------|--------------|-------|-------|
| | Analysis | 30-hr | 54-hr | Analysis | 24-hr | 48-hr | Analysis | 24-hr | 48-hr |
| $T_{\text{ground-FC}}$ | -0.2 | -0.2 | -0.4 | 0.0 | -0.6 | -0.8 | -1.5 | -0.8 | -1.0 |
| 1-STD | 1.6 | 1.9 | 2.0 | 1.3 | 2.1 | 2.5 | 1.8 | 2.3 | 2.5 |
| RMSE | 1.6 | 1.9 | 2.0 | 1.3 | 2.2 | 2.7 | 2.3 | 2.5 | 2.7 |

Figure Captions

[Figure 1](#). Overview of the study region based on the RGB Aqua MODIS overpass of June 29th, 2015 with marking of study domains (yellow boxes) and states referred to in the text. Also marked in red are Terra and Aqua fire hotspot detections for that day.

Formatted: Font: Bold

[Figure 12](#). Overview of the June 29th burning event. (a)-(d) MODIS Terra RGB with daily combined MODIS active fire hot spot detections for June 27-30. (e) Timeseries of AERONET fine mode τ_{500} , sites marked 1-4 indicated on (a)-(d).

[Figure 2-3](#) (a), (c), (e) True color images of a smoke event over the Midwestern US (June 28, 29, 30, 2015, respectively), constructed using the Level 1b Terra MODIS data overlaid are the ASOS 18:00Z ASOS temperatures. Core evaluation sites are labeled; (b), (d), (f) with corresponding 550 nm aerosol optical thickness from the Collection 6 Terra MODIS aerosol products; (g) and (h), mean 18:00Z station temperature +/- 15 days of the event (June 15- July 14, 2015. June 29 data are excluded for constructing [Figure 3-2g](#) and June 30 data are excluded for constructing [Figure 3-2h](#)).

[Figure 34](#). ECMWF Reanalysis of 700 hPa geopotential heights overlaid on winds for June (a) 28, (b) 29, and (c) 30, 2015 at 18:00Z.

[Figure 45](#). Radiosonde release for Aberdeen, South Dakota for June 29, 12:00Z (solid) and June 30, 00:00Z (dashed).

[Figure 56](#). The forecasted daily maximum temperatures from Grand Forks and Bismarck National Weather Service offices as a function of forecasting hours. Stars represent observed daily maximum temperature for the two stations on June 29, 2015.

[Figure 67](#). (a) The observed near surface air temperature and (b) The differences in observed and ECWFM 30-hour forecasted near surface air temperature (ΔT_{30h}) as a function of MODIS DT τ_{550} for both the June 29th and the June 30th case. (c) RGB image over the upper Midwest on June 29th, 2015, constructed using Terra MODIS level 1B data. Over-plotted on [Figure 7-6c](#) are ΔT_{30h} values from each ASOS station. (d) Similar to (c) but over the Ohio River Valley on June 30th, 2015.

[Figure 78\(a\)-\(c\)](#). 0-, 30- and 542-hour forecasts of 2-m air temperatures for the study region as shown in [Figure 3-2a](#) at 18:00UTC, June 29, 2015 from ECMWF model runs. (d-f). The differences between ECMWF modeled 2-m temperatures (at 18:00UTC, June 29, 2015) and surface observations (using ground stations as shown in [Figure 3-2c](#)) as a function of Collection 6 Terra MODIS DT τ_{550} . Data pairs are colored based on the observed monthly mean surface temperatures at 18:00UTC as shown in [Figure 3-2g](#). Data pairs for regions with monthly mean temperatures of < 22°C, in between 22°C and 24.5°C and > 24.5°C are colored in blue, green and red respectively. Red dash lines are the linear fit lines to the data pairs with red colors, and green dash lines are the linear fit lines for data pairs with green colors.

Figure 89. (a) Yearly averaged, $0.5 \times 0.5^\circ$ (Latitude/Longitude) binned τ_{550} from the Collection 6 Aqua and Terra MODIS combined DT and DB aerosol products for 2014; (b) The number of days with daily mean MODIS τ_{550} larger than 1 for a given $0.5 \times 0.5^\circ$ (Latitude/Longitude) bin; (c) The number of cases when an absolute change in daily MODIS τ_{550} of above 1 is detected from two contiguous days for a given $0.5 \times 0.5^\circ$ (Latitude/Longitude) bin.

Figure A1. (a)-(c). 0-, 24- and 48-hour forecasts of 1.5-m air temperatures for the study region as shown in Figure 32a at 18:00UTC, June 29, 2015 from UKMO model runs. (d-f). The differences between UKMO modeled 2-m temperatures (at 18:00UTC, June 29, 2015) and surface observations (using ground stations as shown in Figure 32c) as a function of Collection 6 Terra MODIS DT τ_{550} . Data pairs are colored based on the observed monthly mean surface temperatures at 18:00UTC as shown in Figure 32g. Data pairs for regions with monthly mean temperatures of $< 22^\circ\text{C}$, in between 22°C and 24.5°C and $> 24.5^\circ\text{C}$ are colored in blue, green and red respectively. Red dash lines are the linear fit lines to the data pairs with red colors, and green dash lines are the linear fit lines for data pairs with green colors.

Figure A2. (a)-(c). 0-, 24- and 48-hour forecasts of 2-m air temperatures for the study region as shown in Figure 32a at 18:00UTC, June 29, 2015 from NCEP model runs. (d-f). The differences between NCEP modeled 2-m temperatures (at 18:00UTC, June 29, 2015) and surface observations (using ground stations as shown in Figure 32c) as a function of Collection 6 Terra MODIS DT τ_{550} . Others are similar as Figure A1.

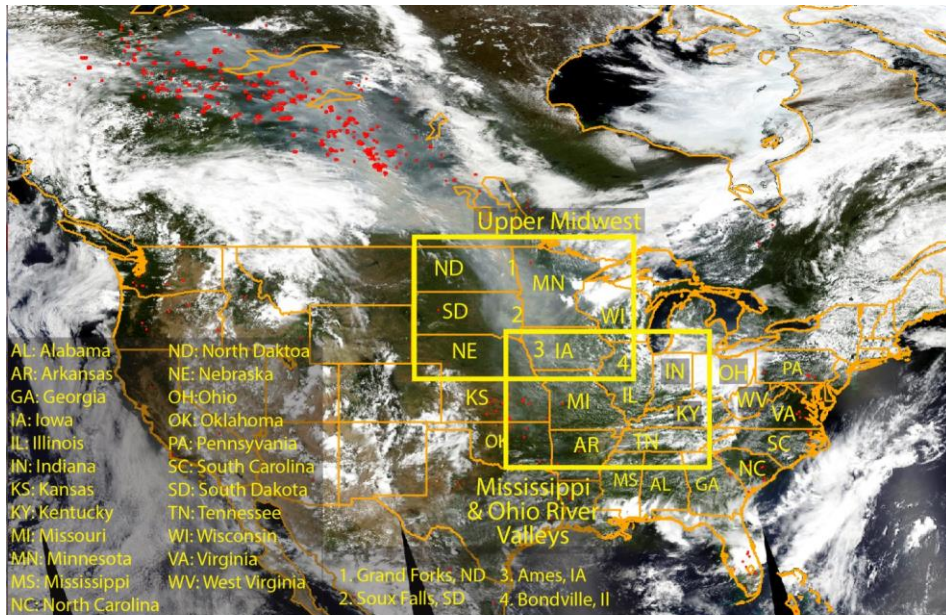


Figure 1. Overview of the study region based on the RGB Aqua MODIS overpass of June 29th, 2015 with marking of: study domains (yellow boxes); states referred to in the text.; and numbered locations of key AERONET sites used in the analysis. Also marked in red are Terra and Aqua fire hotspot detections for this day.

Formatted: Superscript

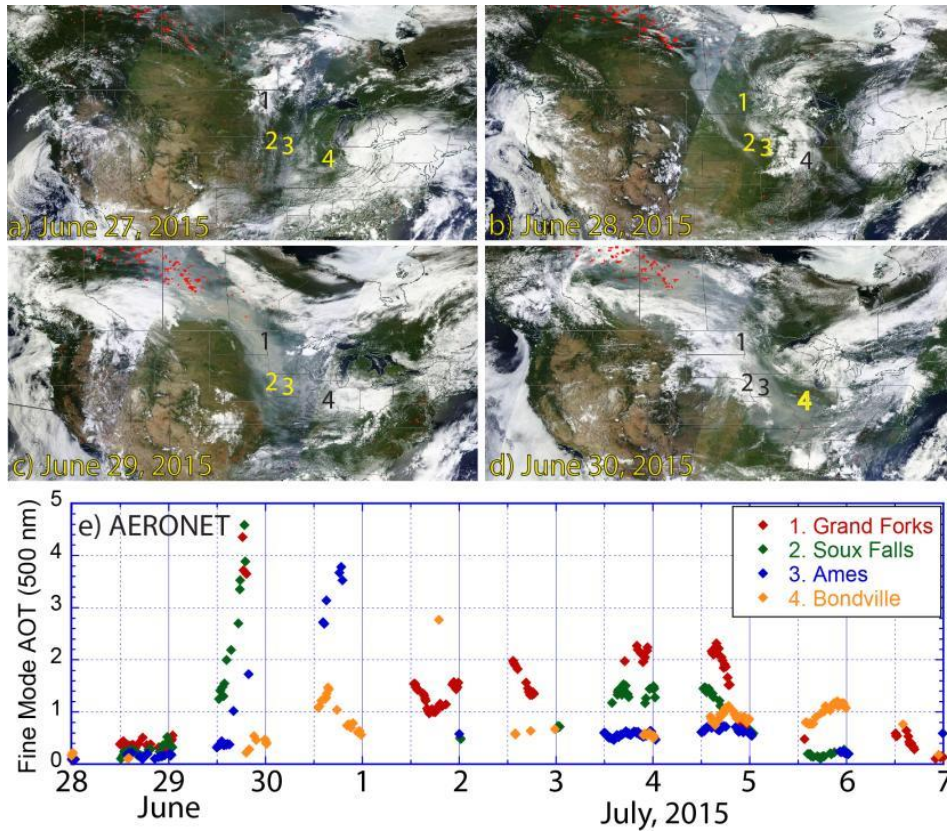


Figure 12. Overview of the June 29th burning event. (a)-(d) MODIS Terra RGB with daily combined MODIS active fire hot spot detections for June 27-30. (e) Timeseries of AERONET fine mode τ_{500} , sites marked 1-4 indicated on (a)-(d).

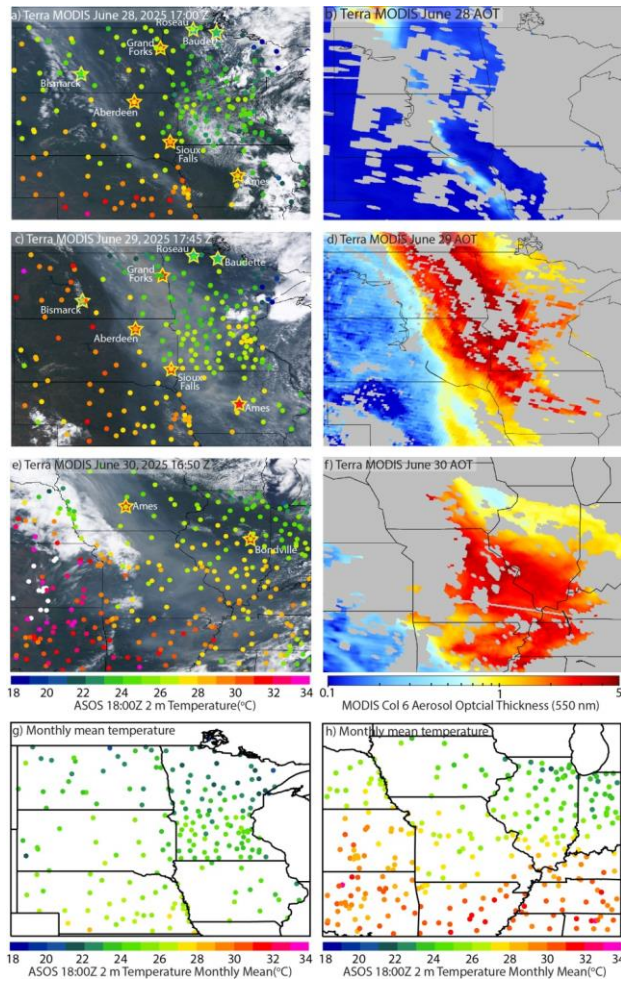


Figure 2-3 (a), (c), (e) True color images of a smoke event over the Midwestern US (June 28, 29, 30, 2015, respectively), constructed using the Level 1b Terra MODIS data. Overlaid are the ASOS 18:00Z ASOS temperatures. Core evaluation sites of are labeled; (b), (d), (f) Corresponding 550 nm aerosol optical thickness from the Collection 6 Terra MODIS aerosol products; (g) and (h), mean 18:00Z station temperature +/- 15 days of the event (June 15- July 14, 2015). June 29 data are excluded for constructing [Figure- 32g](#) and June 30 data are excluded for constructing [Figure- 32h](#)).

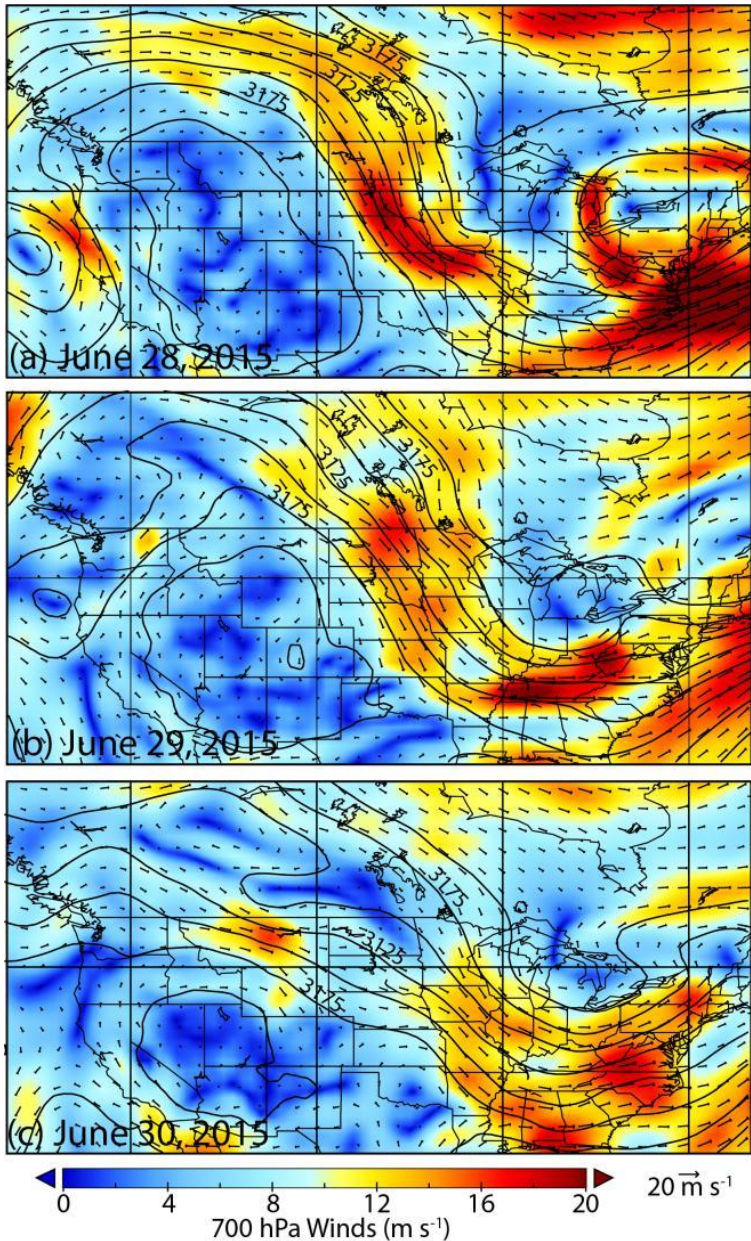


Figure 34. ECMWF Reanalysis of 700 hPa geopotential heights overlaid on winds for June (a) 28, (b) 29, and (c) 30, 2015 at 18:00Z.

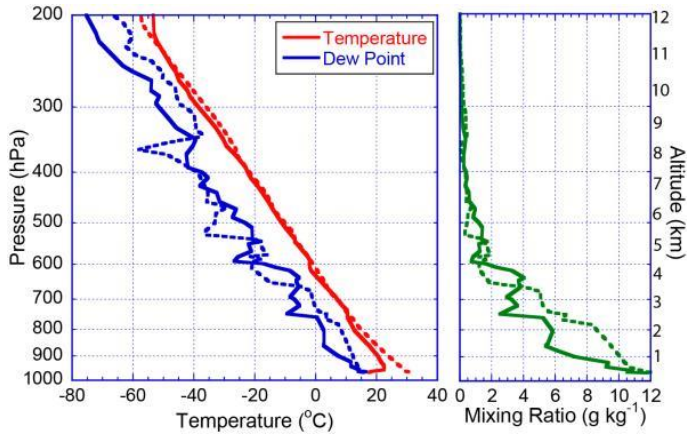


Figure 45. Radiosonde release for Aberdeen South Dakota for June 29, 12:00Z (solid) and June 30, 00:00Z (dashed).

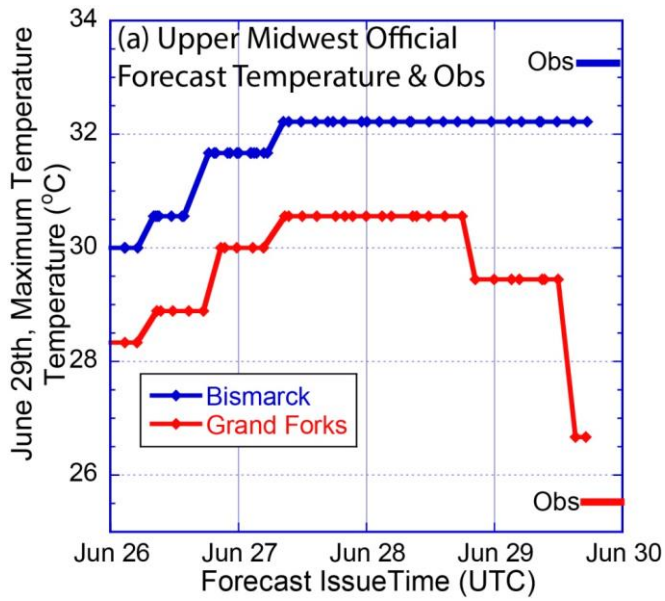


Figure 56. The forecasted daily maximum temperatures from Grand Forks and Bismarck National Weather Service offices as a function of forecasting hours. Stars represent observed daily maximum temperature for the two stations on June 29, 2015.

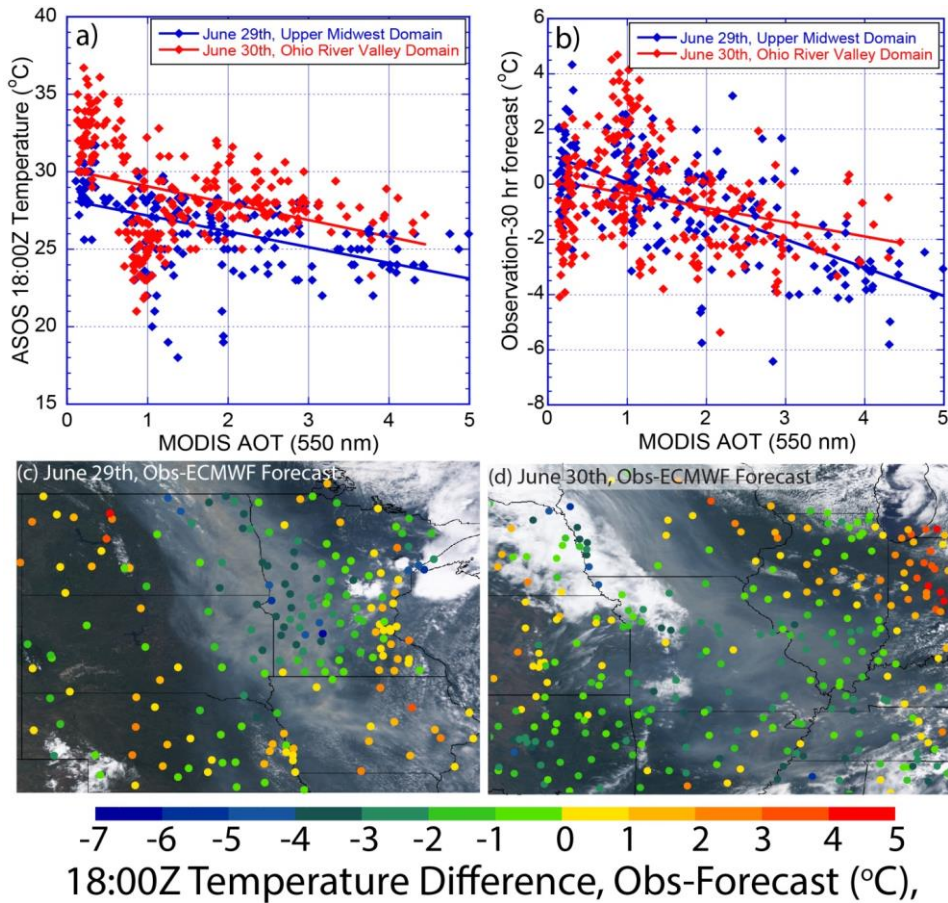


Figure 67. (a) The observed near surface air temperature and (b) The differences in observed and ECWmf 30-hour forecasted near surface air temperature (ΔT_{30h}) as a function of MODIS DT τ_{550} for both the June 29th and the June 30th case. (c) RGB image over the upper Midwest on June 29th, 2015, constructed using Terra MODIS level 1B data. Over-plotted on Figure 76(c) are ΔT_{30h} values from each ASOS station. (d) Similar to (c) but over the Ohio River Valley on June 30th, 2015.

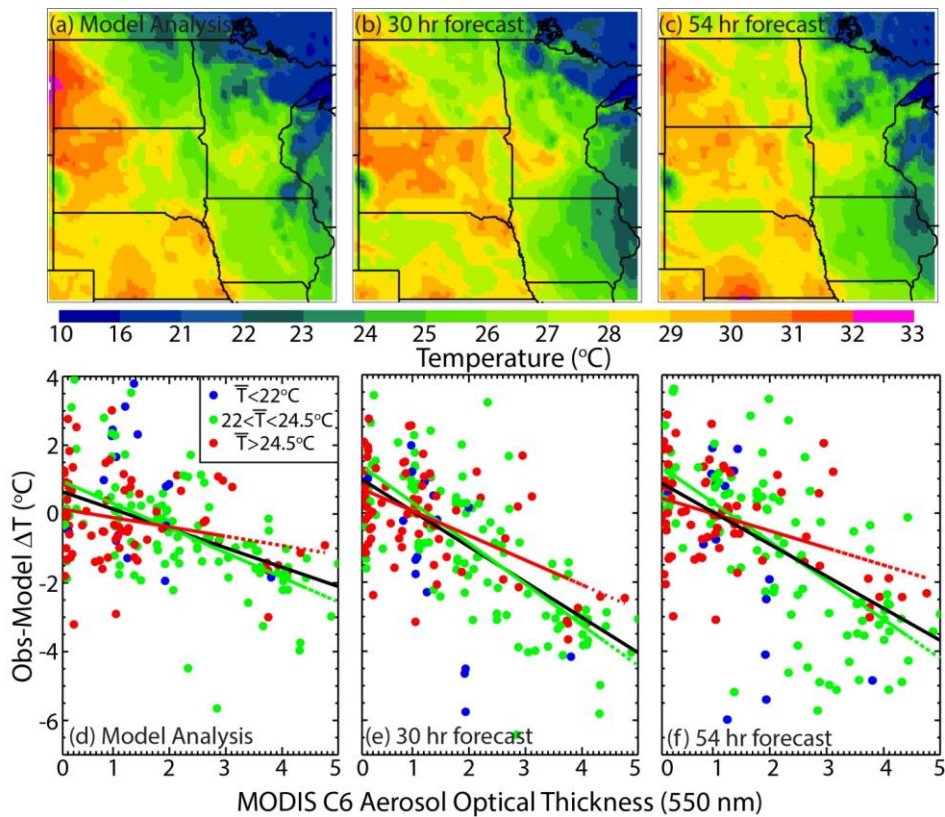


Figure 7a8a-c). 0-, 30- and 54-hour forecasts of 2-m air temperatures for the study region as shown in Figure 32a at 18:00UTC, June 29, 2015 from ECMWF model runs. (d-f). The differences between ECMWF modeled 2-m temperatures (at 18:00UTC, June 29, 2015) and surface observations (using ground stations as shown in Figure 32c) as a function of Collection 6 Terra MODIS DT τ_{550} . Data pairs are colored based on the observed monthly mean surface temperatures at 18:00UTC as shown in Figure 32g. Data pairs for regions with monthly mean temperatures of $< 22^\circ\text{C}$, in between 22°C and 24.5°C and $> 24.5^\circ\text{C}$ are colored in blue, green and red respectively. Red dash lines are the linear fit lines to the data pairs with red colors, and green dash lines are the linear fit lines for data pairs with green colors.

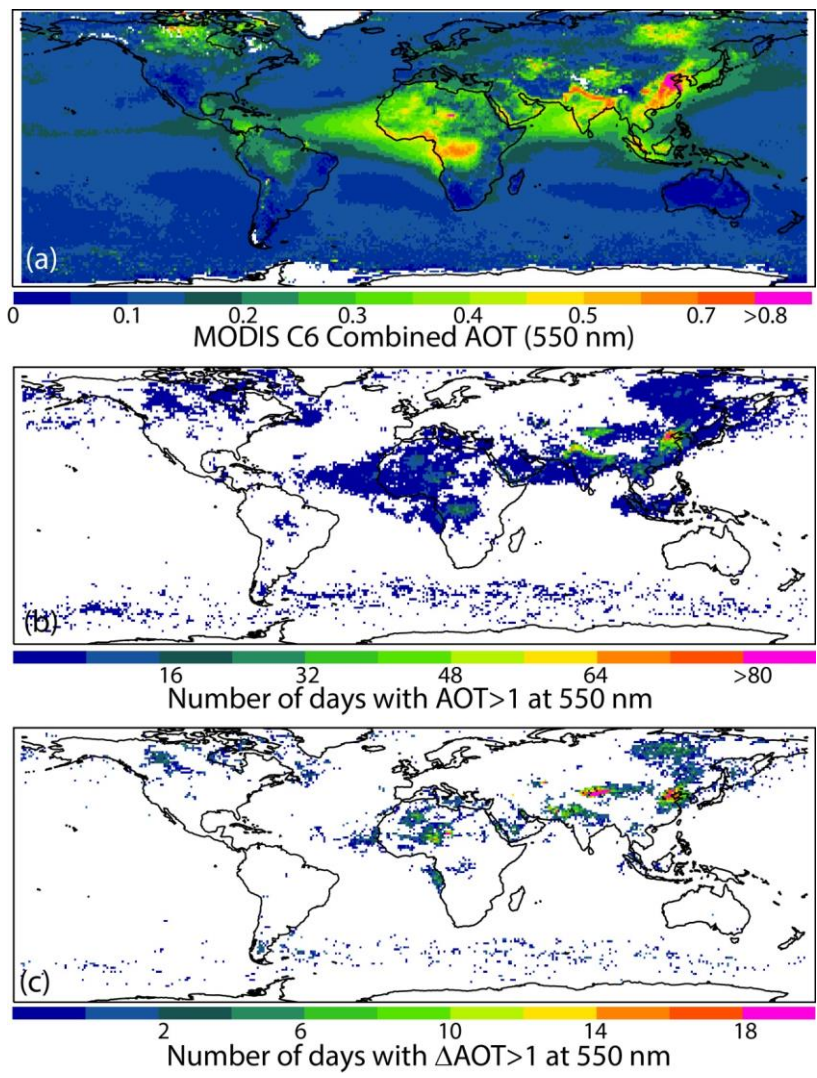


Figure 89. (a) Yearly averaged, $0.5 \times 0.5^\circ$ (Latitude/Longitude) binned τ_{550} from the Collection 6 Aqua and Terra MODIS combined DT and DB aerosol products for 2014; (b) The number of days with daily mean MODIS τ_{550} larger than 1 for a given $0.5 \times 0.5^\circ$ (Latitude/Longitude) bin; (c) The number of cases when an absolute change in daily MODIS τ_{550} of above 1 is detected from two contiguous days for a given $0.5 \times 0.5^\circ$ (Latitude/Longitude) bin.

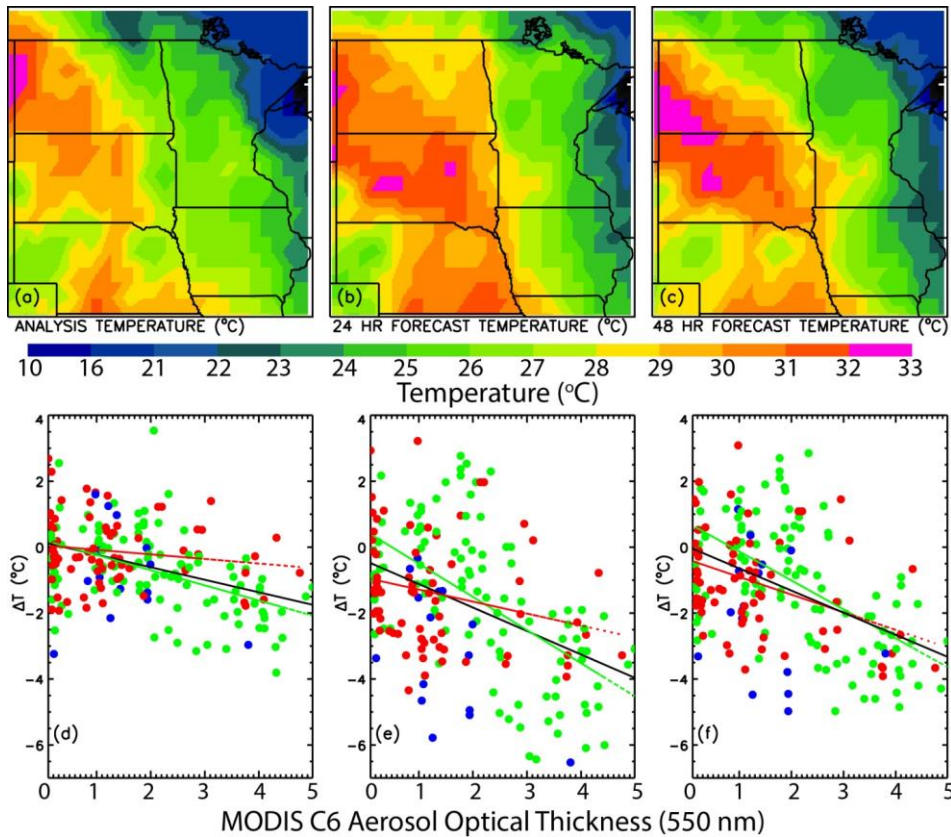


Figure A1. (a)-(c). 0-, 24- and 48-hour forecasts of 1.5-m air temperatures for the study region as shown in Figure 32a at 18:00UTC, June 29, 2015 from UKMO model runs. (d-f). The differences between UKMO modeled 2-m temperatures (at 18:00UTC, June 29, 2015) and surface observations (using ground stations as shown in Figure 32c) as a function of Collection 6 Terra MODIS DT τ_{550} . Data pairs are colored based on the observed monthly mean surface temperatures at 18:00UTC as shown in Figure 32g. Data pairs for regions with monthly mean temperatures of $< 22^\circ\text{C}$, in between 22°C and 24.5°C and $> 24.5^\circ\text{C}$ are colored in blue, green and red respectively. Red dash lines are the linear fit lines to the data pairs with red colors, and green dash lines are the linear fit lines for data pairs with green colors.

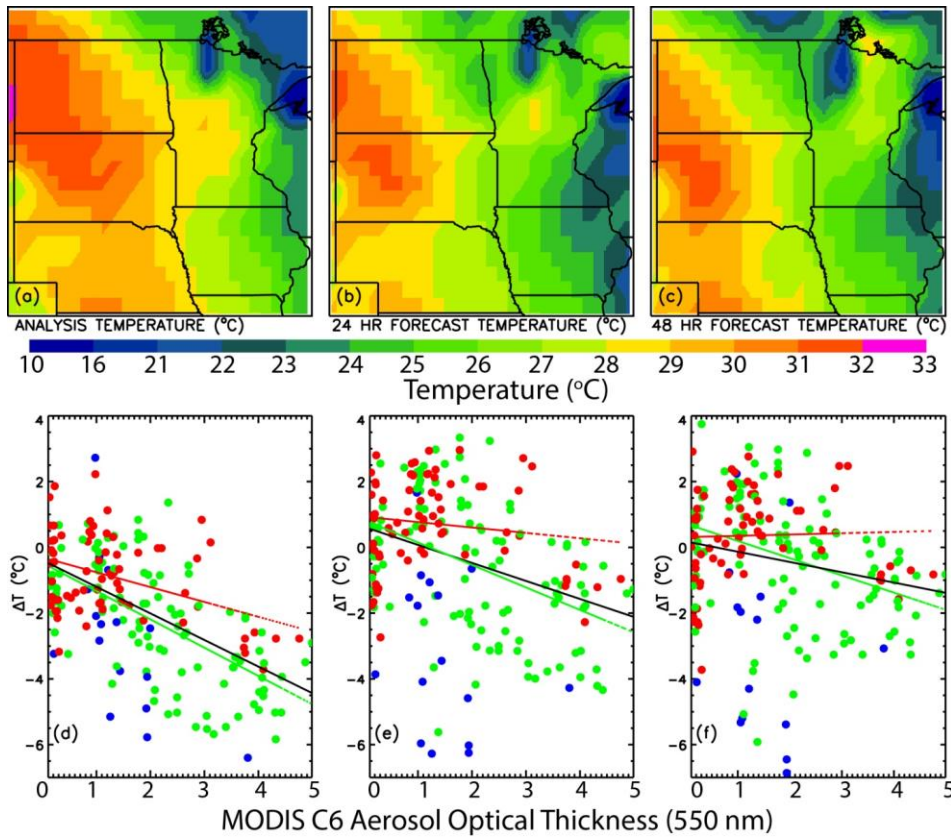


Figure A2. (a-c). 0-, 24- and 48-hour forecasts of 2-m air temperatures for the study region as shown in Figure 32a at 18:00UTC, June 29, 2015 from NCEP model runs. (d-f). The differences between NCEP modeled 2-m temperatures (at 18:00UTC, June 29, 2015) and surface observations (using ground stations as shown in Figure 32c) as a function of Collection 6 Terra MODIS DT τ_{550} . Others are similar as Figure A1.